

Copyright Warning & Restrictions

The copyright law of the United States (Title 17, United States Code) governs the making of photocopies or other reproductions of copyrighted material.

Under certain conditions specified in the law, libraries and archives are authorized to furnish a photocopy or other reproduction. One of these specified conditions is that the photocopy or reproduction is not to be “used for any purpose other than private study, scholarship, or research.” If a user makes a request for, or later uses, a photocopy or reproduction for purposes in excess of “fair use” that user may be liable for copyright infringement,

This institution reserves the right to refuse to accept a copying order if, in its judgment, fulfillment of the order would involve violation of copyright law.

Please Note: The author retains the copyright while the New Jersey Institute of Technology reserves the right to distribute this thesis or dissertation

Printing note: If you do not wish to print this page, then select “Pages from: first page # to: last page #” on the print dialog screen

The Van Houten library has removed some of the personal information and all signatures from the approval page and biographical sketches of theses and dissertations in order to protect the identity of NJIT graduates and faculty.

ABSTRACT

Title of Thesis : Two Dimensional Diffusional Model
for Leakage of Macromolecules in
The Interstitial Space

Suthiluk Dumrongsiri, Master of Science, 1985

Thesis directed by : Dr. David S. Kristol
Dr. Arthur B. Ritter

Two dimensional diffusion of macromolecules through the interstitial in the hamster cheek pouch was studied with intravital fluorescence microscopy. After topical application of Bradykinin, the movement of Fluorescein isothiocyanate (FITC)-labeled dextrans of average molecular weight 150,000 daltons (Dextran 150) was recorded on videotape which latter was played back frame-by-frame for analysis by digital image processing. Leakage of macromolecules in response to topical application of Bradykinin occurs at discrete leakage site in post capillary venules of 15-25 μm diameter, rather than in the capillary themselves. A mathematical model of two dimensional convection plus diffusion was used to simulate the macromolecule transport. The model simulations were compared with the experimental data to estimate interstitial diffusion coefficients and velocities. The model which best fit the experimental data consisted of four discrete leakage points at the origin. The additional of a small interstitial convective component in both the x and y directions gave a better fit of data than did a pure

diffusion model. The apparent diffusion coefficient of FITC-dextran 150 was estimated to be 1.0×10^{-7} cm²/sec. The interstitial velocities on the X- and Y- axes were both the same and estimated as 1.0×10^{-4} cm/sec for the best fit in the interstitial diffusion space of the hamster cheek pouch.

TWO DIMENSIONAL DIFFUSIONAL MODEL
FOR LEAKAGE OF MACROMOLECULES
IN THE INTERSTITIAL SPACE

by

Suthiluk Dumrongsiri

This thesis submitted to the Faculty of the Graduate School
of the New Jersey Institute of Technology in partial
fulfillment of the requirements for the degree of
Master of Science
1985

APPROVAL OF THESIS

TWO DIMENSIONAL DIFFUSIONAL MODEL
FOR LEAKAGE OF MACROMOLECULES IN
THE INTERSTITIAL SPACE

BY

Ms. Suthiluk Dumrongsiri

for

Master of Science

in

THE DEPARTMENT OF BIOMEDICAL ENGINEERING
NEW JERSEY INSTITUTE OF TECHNOLOGY

Thesis Approved By :

Dr. David S. Kristol _____

Date:

5/6/85

Dr. Arthur B. Ritter _____

Date:

5/6/85

Dr. Stanley S. Reisman _____

Date:

5/8/85

VITA

Name : Suthiluk Dumrongsiri
Permanent address :
Degree : BS. , 1981.
Date of birth :
Place of birth :
Primary education : Rajinee Bon School, Bangkok, Thailand
March 1975.
Secondary education : Trium-Udom Suksa School, Bangkok,
Thailand , March 1977.

Collegiate institutions attended	Date	Degree	Date of Degree
Chulalongkorn University	77/81	BS.	5/81.
New Jersey Institute of Technology	82/85	MS.	5/85.

Major : Biomedical Engineering
Position held : Research Assistant, Biomedical
Engineering Department , NJIT.

DEDICATION

I would like to dedicate this thesis to my parents for their support and encouragement, and to Kun Patumraj , for his assistance , guidance , and help throughout my stay in The United States.

ACKNOWLEDGEMENT

I would like to express my sincerest appreciation to my advisor, Prof. Arthur B. Ritter, for all his assistance, help, and friendship throughout this thesis. His enthusiasm and inspiration will always be greatly appreciated.

I would also like to acknowledge Prof. David Kristol for all of his kindness, support and guidance at NJIT.

TABLE OF CONTENTS

Introduction	1
Experimental Procedures :	
Tracer and Animal Preparation	4
Optics and Instrumentation	6
Select Picture Frame and Image Processing	8
Image Program	14
Sagid Program	16
Mathematical Model	22
Computer Model	25
Model Solutions	37
Results :	
Data from The First Experiment	58
Data from The Second Experiment	67
Discussion :	
The Best Fit Model	78
Related Work Done by Others	83
Possible Error Sources	92
Conclusion	94
Appendix A.	95
Main Program	96
Bou Program	100
Coeff Program	102
Sconv Program	103
Reference	105

Lists of Tables

Table of variables meaning	32
Table 3.1. The solution of Model I	40
Table 3.2. The solution of Model II	43
Table 3.3. The solution of Model III	46
Table 3.4. The stability of the solution	57
Table 4.1. The calculated concentration for the graph in Fig.4.4.	63
Table 4.2. The calculated concentration for the graph in Fig.4.4.	64
Table 4.3. The model solution used in Fig.4.4.	65
Table 4.4. The calculated concentration for the graph in Fig.4.6a,b	71
Table 4.5. The model solution used in Fig.4.6a,b	72
Table 4.6. The calculated concentration for the graph in Fig.4.8.	75
Table 4.7. The model solution used in Fig.4.8.	76
Table 5.1. Nakamura's D values	86
Table 5.2. Fox's D values	88
Table 5.3. Nugent's D values	91

Lists of Figures

Fig.1.0. Schematic diagram of the experimental system	7
Fig.1.0.1. The first common point	10
Fig.1.0.1(a,b,c). The area of interest	11
Fig.1.0.2. The second common point	12
Fig.1.0.2(a,b). The area of interest	13
Fig.1.4. Blockdiagram of program IMAGE	15
Fig.1.1. Grayscale distribution (53 sec)	19
Fig.1.2. Grayscale distribution (105 sec)	20
Fig.1.3. Grayscale distribution (31 sec)	21
Fig.3a. Flow-diagram of "MAIN"	27
Fig.3b. Flow-diagram of "RUNGE"	28
Fig.3c. Flow-diagram of "COEFF"	34
Fig.3d. Flow-diagram of "BOU"	35
Fig.3e. Flow-diagram of "SCONV"	36
Fig.3.1. Model I	39
Fig.3.2. Curves of Model I	41
Fig.3.3. Model II	42
Fig.3.4. Curves of Model II	44
Fig.3.5. Model III	45
Fig.3.6. Curves of Model III	47
Fig.3.7a. Diffusion on x-axis	50
Fig.3.7b. Diffusion on y-axis	51
Fig.3.8. 3-Middle leakage model	52
Fig.3.9. Different D coefficient	53

Fig.3.10a. Different V_x, V_y	54
Fig.3.10b. Different V_x, V_y	55
Fig.4.1. The first subregion	60
Fig.4.2. The second subregion	61
Fig.4.3. The best fit model	62
Fig.4.4. Comparison curves	66
Fig.4.5a. The first subregion from Fig.1.3.	69
Fig.4.5b. Distance between pixels	69
Fig.4.6a. Diffusion on y-axis	73
Fig.4.6b. Diffusion on x-axis	74
Fig.4.7. The second subregion from Fig.1.3.	70
Fig.4.8. Comparison curves	77
Fig.5.1. Experimental curves	79
Fig.5.2. Different D, V_x, V_y	85

INTRODUCTION

Transmural exchange of solutes between the blood and tissue as well as interstitial transport of these solutes are important factors in determining the availability of nutrients for utilization by cells. The most important physical parameters contributing to solute movement are the transmural hydrostatic pressure gradient and the concentration gradients across the vessel wall and within the tissue. In a biological system, this process is further complicated both by the structural and functional characteristics of the blood-tissue barrier, and by the physicochemical properties of the material concerned. Intravital microscopy employing tracer techniques and topical applications of vasoactive agents such as bradykinin and histamine have been used to investigate macromolecular transport in the microcirculations of the hamster cheek pouch and rat mesentery. The major conclusions which are important to this study are (ref.5) :

- (1). leakage of macromolecules occurs primarily at discrete leakage sites on post capillary venules of 15-25 um diameter, rather than at true capillaries
- (2). leakage is transient and stops within 15 minutes
- (3). the same leakage sites respond to repeat doses
- (4). there is an increase in the number of sites with increasing dose.

In this thesis experimental macromolecular leakage data obtained in the hamster cheek pouch microcirculation is compared with the solution of a two-dimensional diffusional model using digital video image analysis techniques. The model allows estimation of the interstitial diffusion coefficient of FITC-dextran 150 and the values of interstitial velocities along the x- and y-axes also. Estimates of these parameters in response to challenges by vasoactive substances such as Bradykinin and Platelet Activating Factor (PAF), contribute to better understanding of the mechanisms responsible for macromolecular transport and microvascular wall repair during inflammatory conditions.

EXPERIMENTAL PROCEDURES

Tracer and Animal Preparation :

Male, Syrian hamsters weighing between 80 and 120 g were anesthetized with sodium pentobarbital (60 mg/kg).

A heating pad controlled by a thermistor maintained body temperature at 37°C. A tracheal cannula was inserted. The femoral vein was cannulated for the administration of fluorochrome and supplementary doses of anaesthesia (30 mg/kg).

The hamster cheek pouch was prepared for direct intravital microscopic observation in a manner similar to that previously described by Duling (1973), and Svensjo et al. (1978) (ref.5). The hamster was positioned on a Lucite board provided with a circular viewing pedestal (1 cm diameter) surrounded by a well filled with silicone rubber. The pouch was everted, fashioned into a single layer, and cleared of loose connective tissue. Five or six pins secured the pouch to the silicone rubber. The preparation was subsequently placed on a microscope stage.

During and following eversion of the cheek pouch, a bicarbonate buffer solution continually suffused the tissue. Suffusion was only interrupted for topical application of bradykinin. The millimolar composition of the buffer solution was 131.9 NaCl, 4.7 KCl, 2.0 CaCl₂, 1.2 MgSo₄, and 18.0 NaHCO₃. The suffusion solution was maintained at 35°C.

Fluorescein isothiocyanate (FITC)-dextran 150 (150,000 MW, Pharmacia Fine Chemicals, Uppsala, Sweden) was used to assay microvascular permeability to macromolecules. The FITC-dextran was prepared as a 5% solution in bicarbonate buffer and administered at a dose of 100 mg/kg.

In the first experiment Bradykinin triacetate (Sigma Chemical Co.) was dissolved in bicarbonate buffer and applied topically to the microcirculation of the cheek pouch for a period of 5 min. A concentration of 1.6×10^{-7} M was used.

In the second experiment, Platelet Activating Factor (PAF) (Sigma Company) was dissolved in bicarbonate buffer and applied topically to the microcirculation of the cheek pouch for a period of 3 min. A concentration of 1×10^{-6} M was used.

After the application time (5 min, or 3 min), the Bradykinin and PAF solutions were removed with a syringe and the pouch was again suffused with bicarbonate buffer. The zero time in these experiments corresponds to the time in which the active agents were removed, since no microscopic observations are possible during application and removal.

Optics and Instrumentation :

Observations were made with an Olympus BH microscope equipped with both bright-field transillumination and epi-illumination using 6.3x, 10x, 20x, and 32x long-working distance objectives with 10x oculars. A Ploem vertical illumination system was employed for fluorescent microscopy. Epi-illumination was provided by a 100-W mercury DC lamp source in conjunction with an Olympus FITC exciter filter (488 nm), an Olympus dichroic mirror (DM-500 and O-515), and an Olympus)-515 barrier filter. The recording system was comprised of a Cohu 4410 SIT-TV camera coupled to an RCA TV monitor and a V02800 Sony video recorder.

This Page Intentionally Left Blank

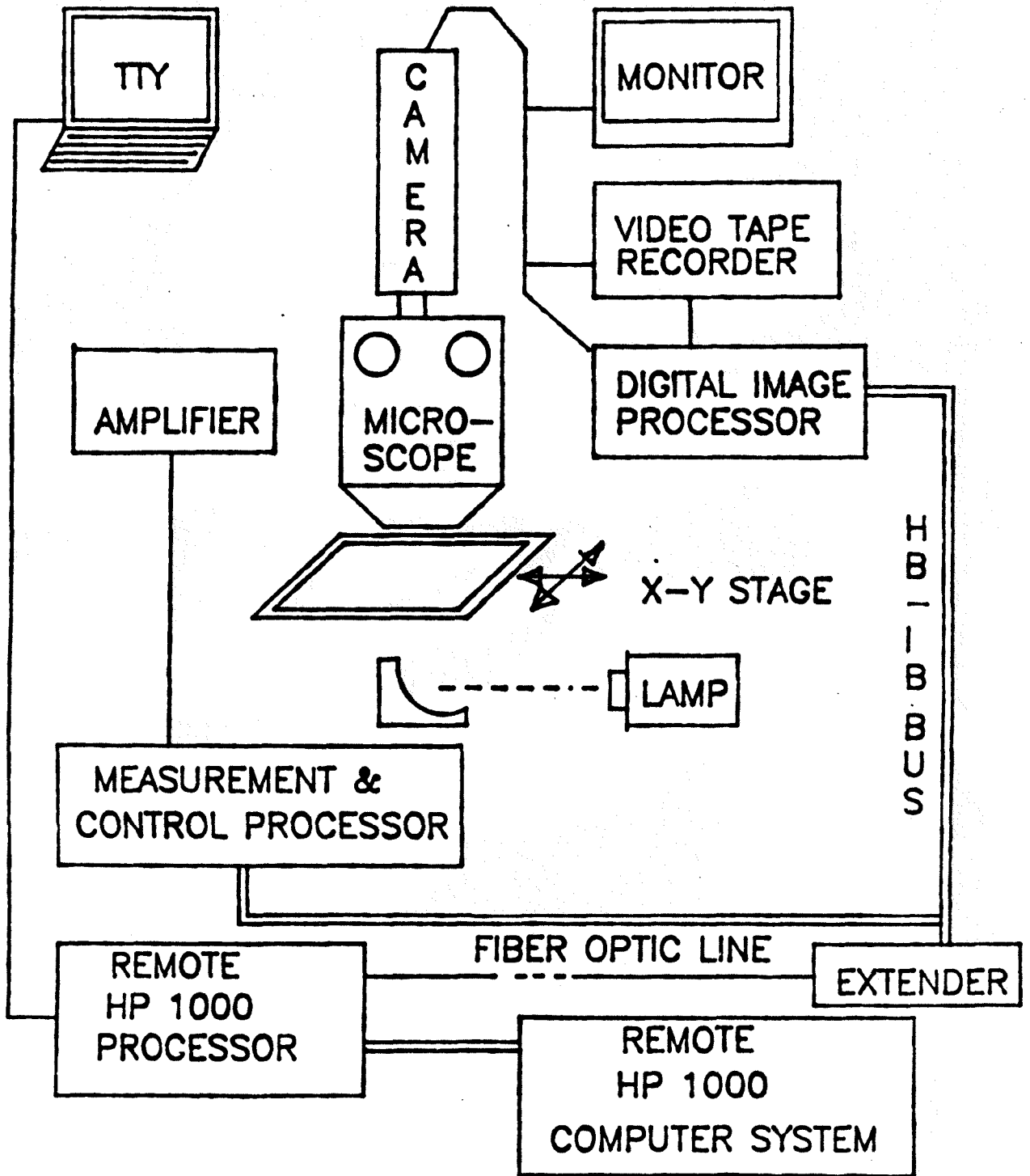


Fig.10. Schematic Diagram of the Experimental System

PICTURE SELECTION AND IMAGE PROCESSING :

A real time playback of the video record of each experiment permitted the selection of frames for detailed analysis. Three frames were selected from the first video tape, then played back on the videotape recorder in single frame mode to get the smaller subregions of 150 by 150 pixels that were later transcribed into digital form from each frame. Because those three subregions were subtracted from each other, they had to be positioned exactly since the software performed a pixel-by-pixel subtraction. The position of a common point which appeared in each subregion was determined exactly. This is shown in Fig.1.0(1). The spot in the middle of the vessel above the area of interest was used as a common focal point; the 150 by 150 areas were all expanded from that spot. The first 150 by 150 subregion shown in Fig.1.0(1a) represents the control-time (before application of Bradykinin or PAF) picture of the area of interest. And in Fig.1.0(1b,c) are the pictures of that area of interest at time 53 and 105 second after removal of the bradykinin solution. The computer mapping showed in Fig.1.1 is the result of the subtraction between (a) and (b) and represents the graycolor intensity of the FITC as a result of diffusion which occurred during 53 second. Similarly, Fig.1.2 is the result of subtraction between (a) and (c) ; the intensity profile due to macromolecular diffusion for 105 seconds.

The same procedure was applied to the second videotape get two subregions of 100 by 100 pixels ,Fig.1.0(2a,b), both subregions were digitized and then subtracted each other giving the intensity profile shown in Fig.1.3. This represents the distribution of graycolor intensity in the interstitial space after 31 second of the diffusion of FITC-dextran 150.

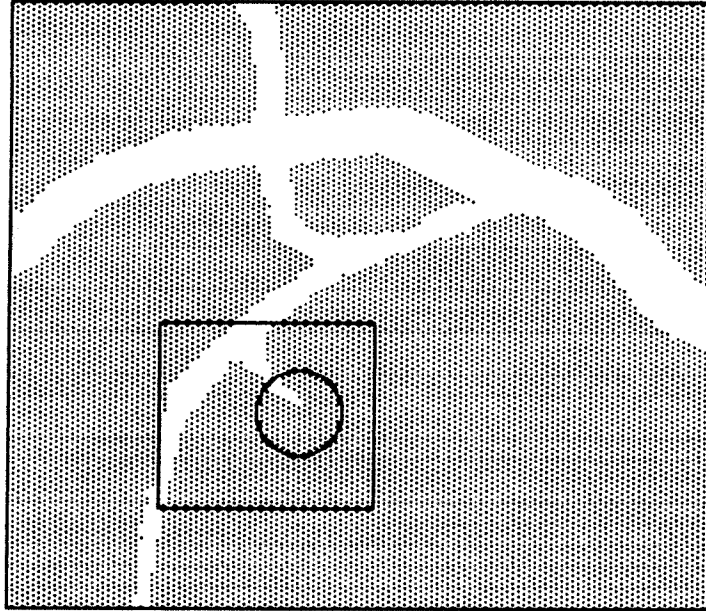


Fig.1.0.1. Point (a) was selected to be the common point of the subregion selected from the first videotape. After the address of (a) was determined, the 150x150 area was expanded from point (a) as shown by the small arrows.

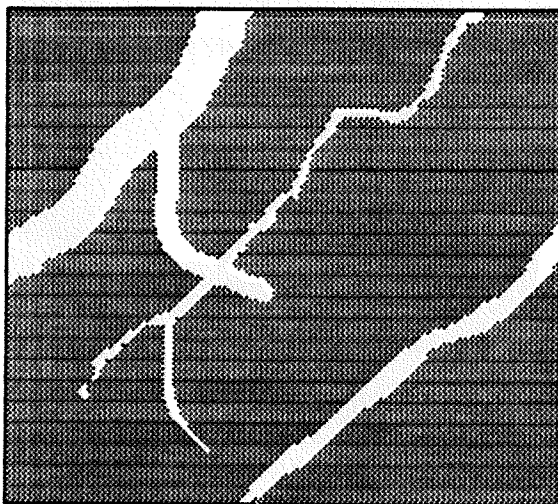


Fig.1.0.1(a). The area of interest at control time (before application of PAF).

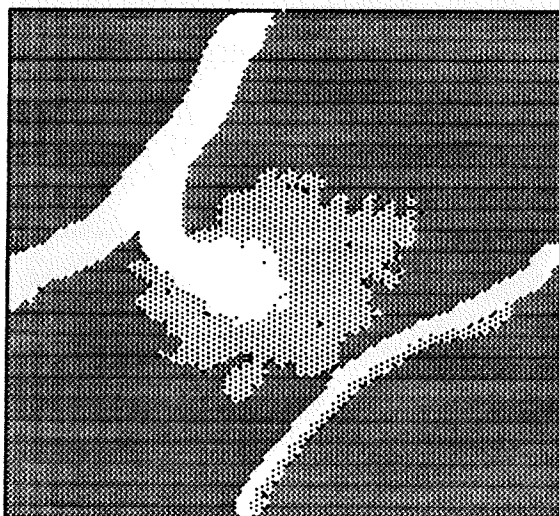


Fig.1.0.1(b). The area of interest at time 53 seconds after removal of PAF.

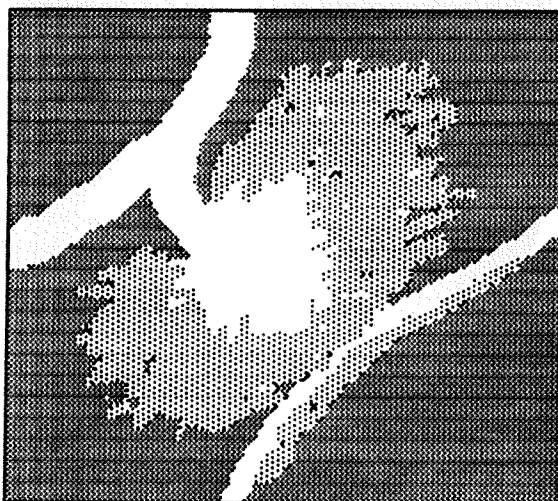


Fig.1.0.1(c). The area of interest at time 105 seconds after removal of PAF.

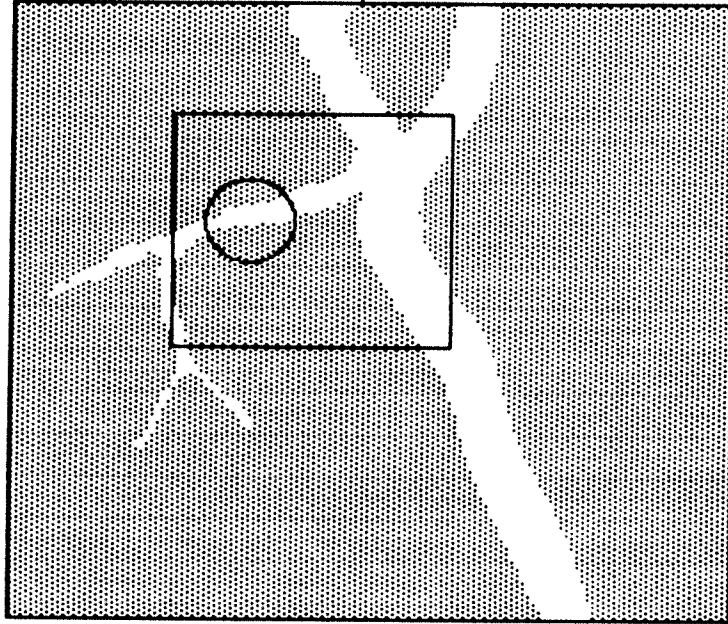


Fig.1.0.2 The subregion which was selected and its common spot is shown.

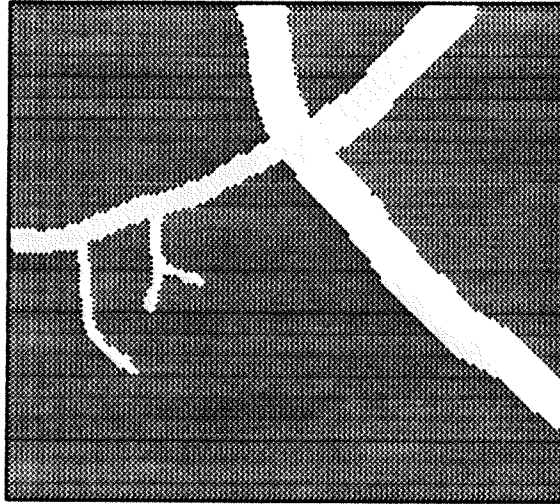


Fig.1.0.2(a). The area of interest at control time.

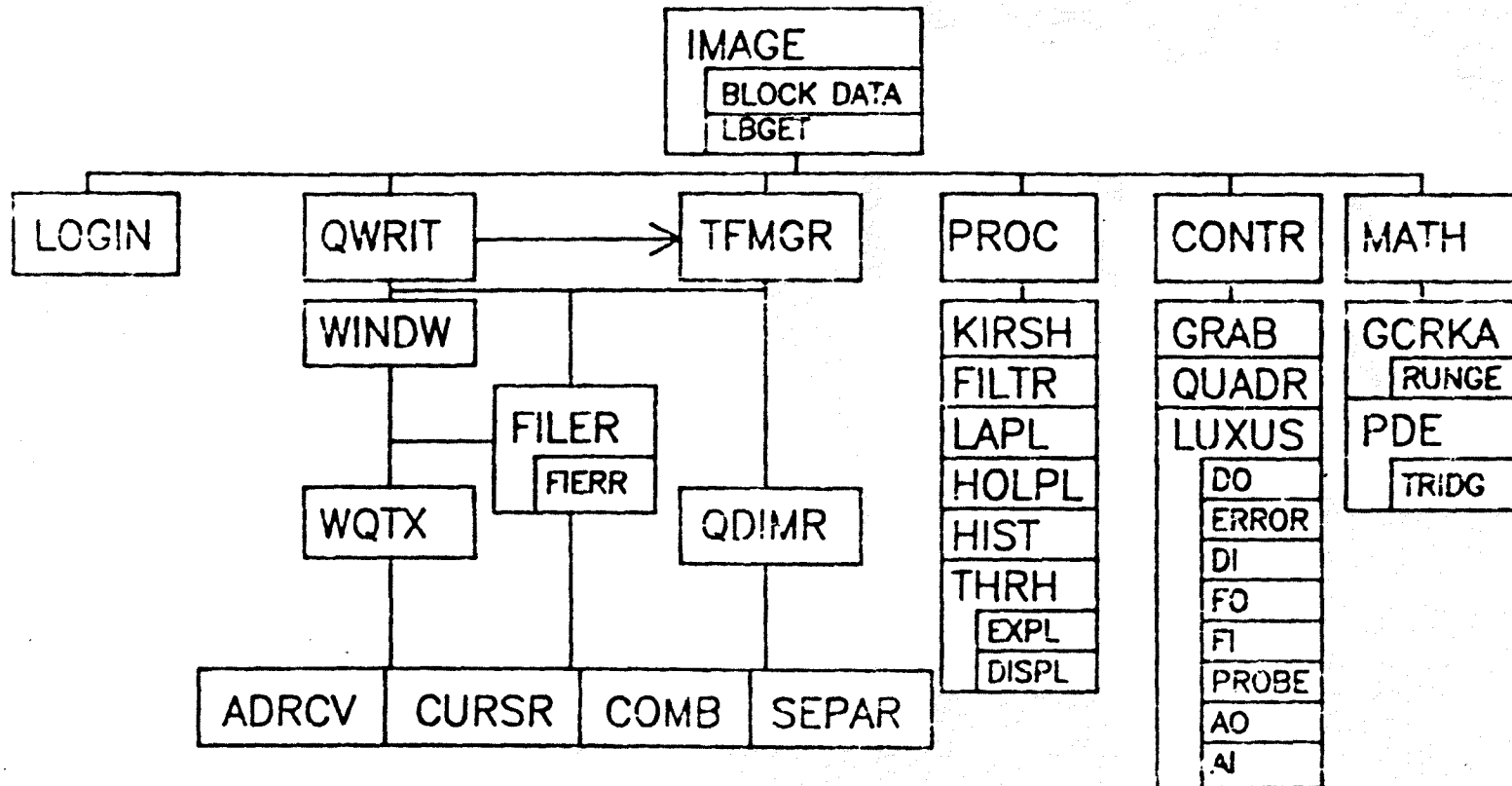


Fig.1.0.2(b). The area of interest at time 31 seconds after removal of Bradykinin.

The digitization of each video frame is accomplished in real time by a video image digitizer (Quantex Corp.). The reading and writing of the graycolor arrays to and from the digitizer memory as well as the subtraction processing were done by the software incorporated into a computer program called "IMAGE".

PROGRAM IMAGE :

Fig.1.4 shows the blockdiagram of program IMAGE. The subregion selected from the frame of videotape was digitized into arrays of picture elements (called "pixels") and stored in a file in digital form on a hard disk. This digital datafile could be converted to analog form and displayed on a TV monitor through the digitizer memory. The software in program IMAGE directed the digital processing software and I/O operations. Once the data for each subregion was stored in digital form the subtraction processing could be performed by the software in IMAGE.



Blockdiagram of Program IMAGE

Fig.1.4.

PROGRAM SAGID :

To display the digital data as a hard copy; digital plotting software in a computer program called "SAGID". The software in SAGID also permitted expansion of the graylevel values for each picture element to cover the full available grayscale range from 0 to 255 to allow better contrast for display.

Since the digital plotter only had four pens (hence only four distinct colors) rather than 256 grayscale ranges, the software in SAGID provided a datafile for the digital plotter. The results of subtraction processing were separated into 4 groups of arrays of picture element depending on gray level. The graycolor range corresponding to each of the four colors was selected by the user. Results shown in Fig.1.1,1.2,1.3.* In those three mappings background and vessel features have been subtracted out and appear as black (graycolor = 0), and leakage pattern of labeled molecules outside the vessel are represented by red green and blue colors. Corresponding to increasing grayscale intensity.

* Since the color mapping will not be able to produce a good result by a general standard black-and-white photocopy, those four colors; black,red,green,blue; have to be represented by four distinct graylevel from light to dark, respectively.

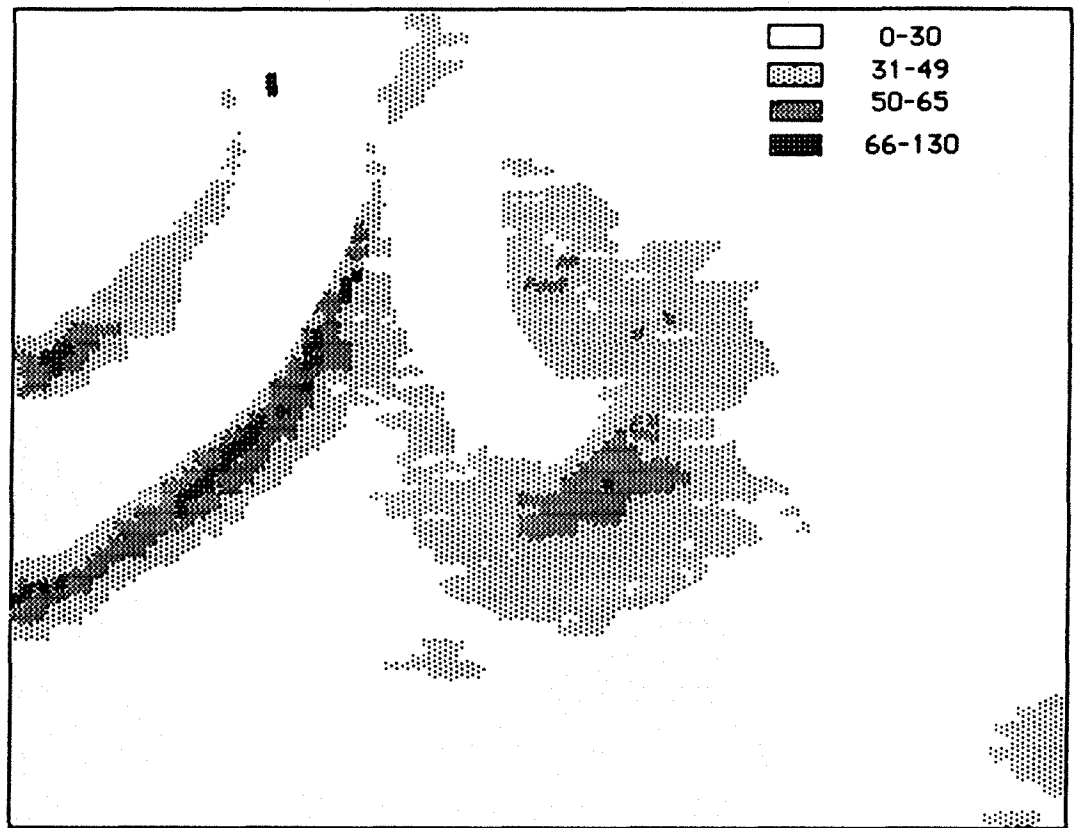
From experiment number one, the output after running program SAGID gave four groups of graycolors which were plotted as :

	range of gray level	color
1	0-30	black
2	31-49	red
3	50-65	green
4	66-130	blue

And from the second experiment, the output of program SAGID was four graycolor ranges corresponding to the following plotter pen colors :

	range of gray level	color
1	0-45	black
2	46-90	red
3	91-135	green
4	136-181	blue

Other software was developed for converting the gray level datafile into concentration of FITC-dextran at each location. A program called "SCONV" performed this task; its blockdiagram and Fortran listing are shown in Fig.3e and in Appendix A, respectively. Use of this program will be discussed in the section on results.



□ □ □ □ represent black, red, green and blue colors.

Fig.1.1. Grayscale distribution around leaking 30 um venule after 53 second of leakage. Leakage of macromolecules caused by topical application of 10^{-5} M Bradykinin for 5 minutes.

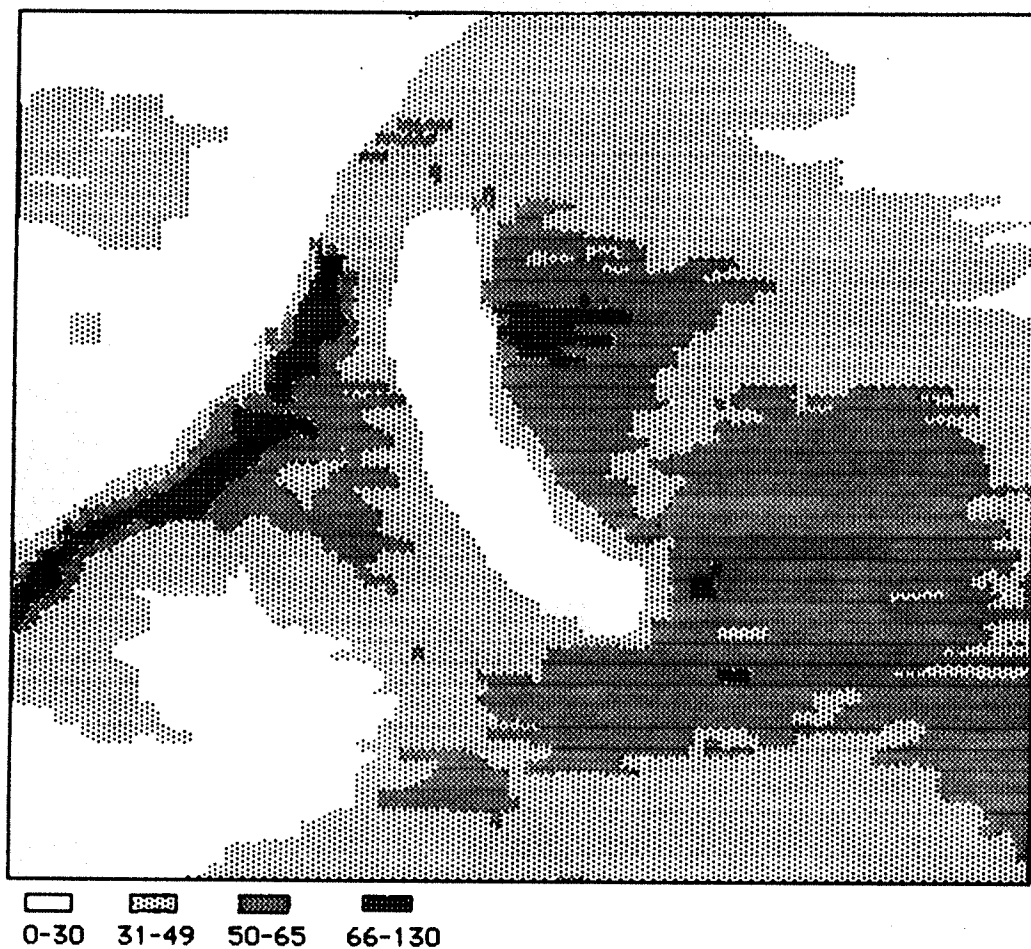


Fig.1.2. Grayscale distribution around leaking 30 um venule after 105 second of leakage. Control grayscale subtracted leakage of macromolecules caused by topical application of 10^{-5} M Bradykinin for 5 minutes.

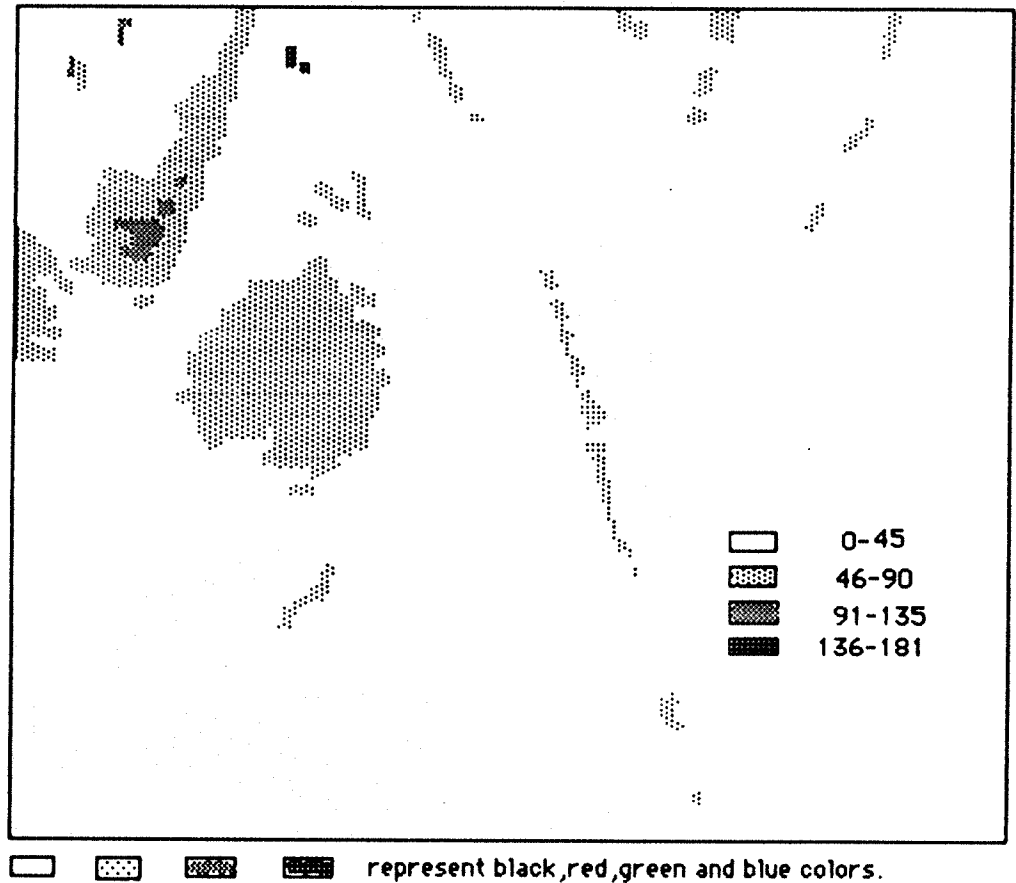


Fig.1.3. Grayscale distribution around leaking 30 μ m venule after topical application of 10^{-5} M Bradykinin for 5 minutes. Leakage pattern with control subtracted 31 second after removal of Bradykinin.

MATHEMATICAL MODEL

Extravasation of FITC-dextran from the leakage site into the interstitial space can be mathematically described by the change of mass concentration of FITC-dextran with respect to time at a fixed point in the X-Y plane, the change resulting from transport of FITC-dextran by convection and diffusion. With the assumption of constant mass density, constant diffusion coefficient, D, and no chemical reaction occurring, this system can be represented by the two-dimensional diffusion equation :

$$\frac{\partial C}{\partial t} + (v_x \frac{\partial C}{\partial x} + v_y \frac{\partial C}{\partial y}) = D(\frac{\partial^2 C}{\partial x^2} + \frac{\partial^2 C}{\partial y^2}) + R \quad (2.1)$$

where x,y are the coordinates perpendicular and parallel to the blood vessel, respectively, t is time, D is the diffusion coefficient in the interstitial space, C is the concentration of FITC-dextran, and R is the reaction rate which equals zero for this system.

To replace the second order spatial derivatives by their finite difference representation, we first expand $C_{(i+1,j)}$ and $C_{(i-1,j)}$ in a Taylor's series around the point $C_{(i,j)}$:

$$C_{(i+1,j)} = C_{(i,j)} + \delta x (\frac{\partial C}{\partial x})_{i,j} + 1/2(\delta x)^2 (\frac{\partial^2 C}{\partial x^2})_{i,j} + \dots \quad (2.2)$$

$$C_{(i-1,j)} = C_{(i,j)} - \delta x (\partial C / \partial x)_{i,j} + 1/2 (\delta x)^2 (\partial^2 C / \partial x^2)_{i,j} + \dots \quad (2.3)$$

Combining eq.(2.2) and (2.3) and solving for $(\partial^2 C / \partial x^2)_{i,j}$:

$$(\partial^2 C / \partial x^2)_{i,j} = (C_{(i+1,j)} - 2C_{(i,j)} + C_{(i-1,j)}) / (\delta x)^2 + O(\delta x)^2 \quad (2.4)$$

$$(\partial^2 C / \partial y^2)_{i,j} = (C_{(i,j+1)} - 2C_{(i,j)} + C_{(i,j-1)}) / (\delta y)^2 + O(\delta y)^2 \quad (2.5)$$

For a very small time step , t, we can represent the time derivative, using Eulers method, as :

$$\partial C_{(i,j,t)} / \partial t \approx (C_{(i,j,t+1)} - C_{(i,j,t)}) / \Delta t \quad (2.6)$$

substituting eq.(2.4),(2.5),(2.6) in eq.(2.1) gives :

$$\begin{aligned} (C_{i,j,t+1} - C_{i,j,t}) / \Delta t = & D((C_{i,j,t} - 2C_{i,j,t} + C_{i-1,j,t}) / (\delta x)^2) \\ & + (C_{i,j+1,t} - 2C_{i,j,t} + C_{i,j-1,t}) / (\delta y)^2 \\ & - v_x (C_{i+1,j,t} - C_{i,j,t}) / \delta x - \\ & v_y (C_{i,j+1,t} - C_{i,j,t}) / \delta y + R \end{aligned} \quad (2.7)$$

Then :

$$\begin{aligned} (C_{i,j,t+1} - C_{i,j,t}) / \Delta t = & a_1 (C_{i+1,j,t} + C_{i-1,j,t}) + a_5 C_{i,j,t} \\ & + a_3 (C_{i,j+1,t} - C_{i,j-1,t}) + b_1 (C_{i,j,t} \\ & - C_{i+1,j,t}) + b_2 (C_{i,j,t} - C_{i,j+1,t}) \end{aligned} \quad (2.8)$$

where $C_{i,j,t}$ = concentration of FITC-dextran at point (x,y) at time t .

$$\begin{aligned}
 a_1 &= (D/(\Delta x)^2) \\
 a_2 &= 2a_1 \\
 a_3 &= (D/(\Delta y)^2) \\
 a_4 &= 2a_3 \\
 a_5 &= -(a_2 + a_3) \\
 b_1 &= v_x/\Delta x \\
 b_2 &= v_y/\Delta y
 \end{aligned} \tag{2.9}$$

The values in eq.(2.9) are called the "coefficients of the model"; since the solution of model depends on the particular values of these coefficients.

The boundary and initial conditions are :

$$\begin{aligned}
 C(i,j,0) &= 0 \text{ for } i \text{ and } j \neq 0 \\
 C(0,0,0) &= C_0(t) \\
 C(\infty, \infty, 0) &= 0 \\
 \partial C(i,b,t)/\partial y &= 0 \\
 \partial C(a,j,t)/\partial x &= 0 \\
 \partial C(0,j,t)/\partial x &= 0 \\
 \partial C(i,0,t)/\partial y &= 0
 \end{aligned}$$

both a and b are distances that are far enough away so that there are no effects from the solution in the region of interest.

COMPUTER MODEL

The mathematical model estimates the change in each grid point with time from the concentration of the surrounding points as :

$$\begin{aligned}
 C(i,j,t+1) = C(i,j,t) + \Delta t & (a_1(C(i-1,j,t)+C(i+1,j,t))+ \\
 & a_5C(i,j,t) + a_3(C(i,j-1,t)+C(i,j+1,t))+ \\
 & b_1(C(i,j,t)-C(i+1,j,t)) + b_2(C(i,j,t)- \\
 & C(i,j+1,t)) + b_3 \qquad \qquad \qquad (3.1)
 \end{aligned}$$

The application of the forth-order Runge Kutta method changes eq.(3.1) to :

$$C(i,j,t+1) = C(i,j,t) + h/6(k_1 + 2Ak_2 + 2Bk_3 + k_4) \quad (3.2)$$

where $h = \Delta t =$ time step change

$$\begin{aligned}
 k_1 &= f(\Delta t, C(i,j,t)) \\
 &= a_1(C(i-1,j,t)+C(i+1,j,t)) + a_5C(i,j,t) + \\
 &\quad a_3(C(i,j-1,t)+C(i,j+1,t)) + b_1(C(i-1,j,t)- \\
 &\quad C(i+1,j,t)) + b_2(C(i,j-1,t)-C(i,j+1,t)) + b_3
 \end{aligned}$$

$$k_2 = f(\Delta t+h/2, C(i,j,t) + hk_1/2)$$

$$k_3 = f(\Delta t+h/2, C(i,j,t) + (-1/2 + 1/\sqrt{2})hk_1+Ahk)$$

$$k_4 = f(\Delta t+h/2, C(i,j,t) - 1/\sqrt{2}hk_2 + Bhk_3)$$

$$A = (1-1/\sqrt{2}) , B = (1+1/\sqrt{2})$$

The error of the fourth-order Runge Kutta method is approximately : $e_t = Kh^5$;where, e_t is the local truncation error and K usually depends upon the function and its higher-order partial derivative in a complicated way (ref.2).

Now the solution can be programmed for calculation by the computer with stability insured by picking the time step, h, such that :

$$h < (\Delta x^2 + \Delta y^2) / 2D$$

(stability requires that $D(1/x^2 + 1/y^2)\Delta t \leq 1/2$).

From eq.(3.2) the flow diagram can be separated into three parts (Fig.3a,3b,3c,3d). Each part was executed by a computer program as shown in Appendix A. The functions of each of the programs were as follows : The program "MAIN" calculates $C(i,j,t+1)$, the final results; the program called "COEFF" calculates the model coefficients, a_i, b_j ; the program called "BOU" defines the initial and boundary conditions. The program called "SCONV" (Fig.3e) converts gray level data to concentration of FITC-dextran by assigning the measured concentration of FITC-dextran in the plasma phase equal to the maximum gray level (255).

Fig. 3a. Flow-diagram of the "MAIN" program.

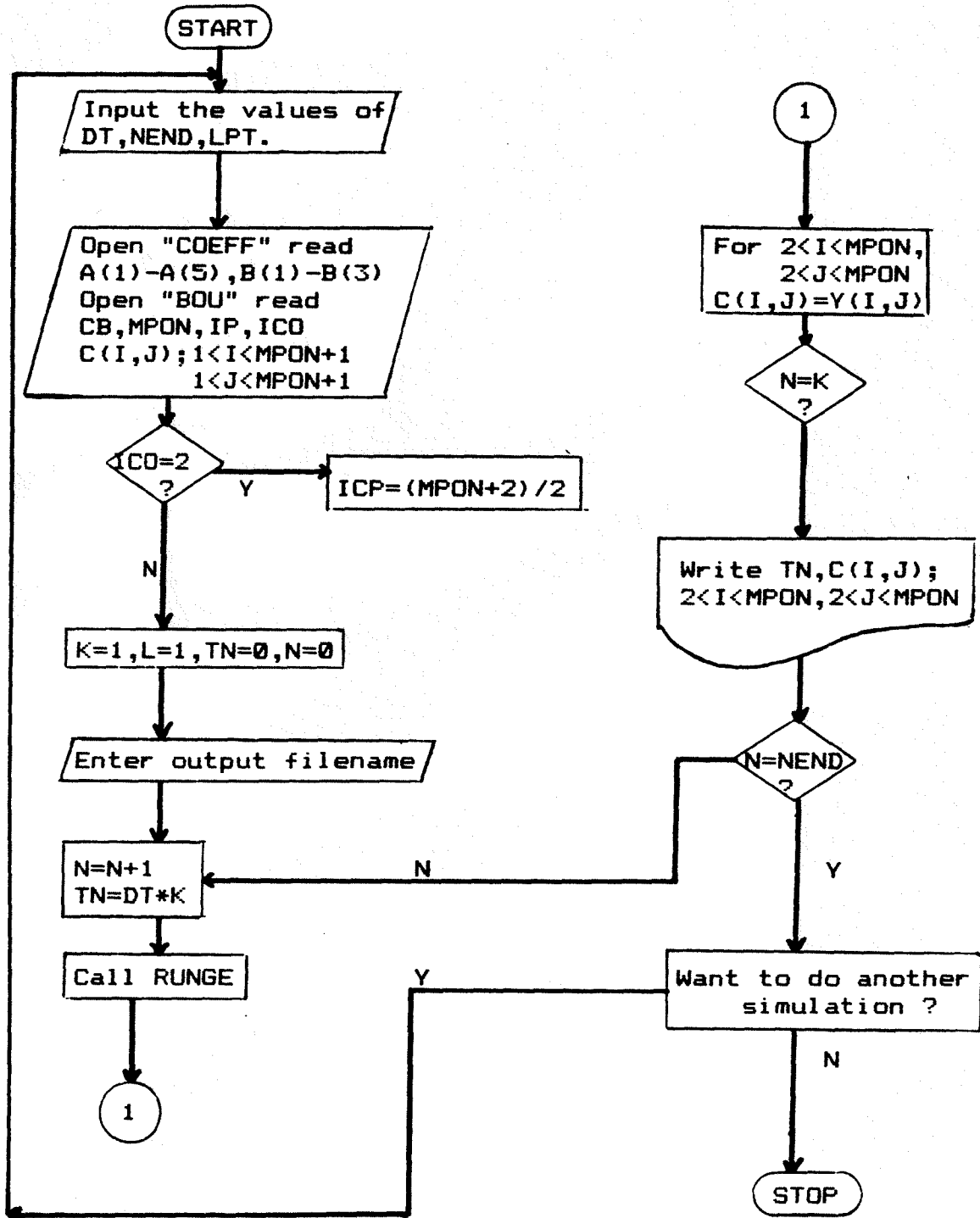


Fig.3b. Flow-diagram of subroutine "RUNGE" of the main program.

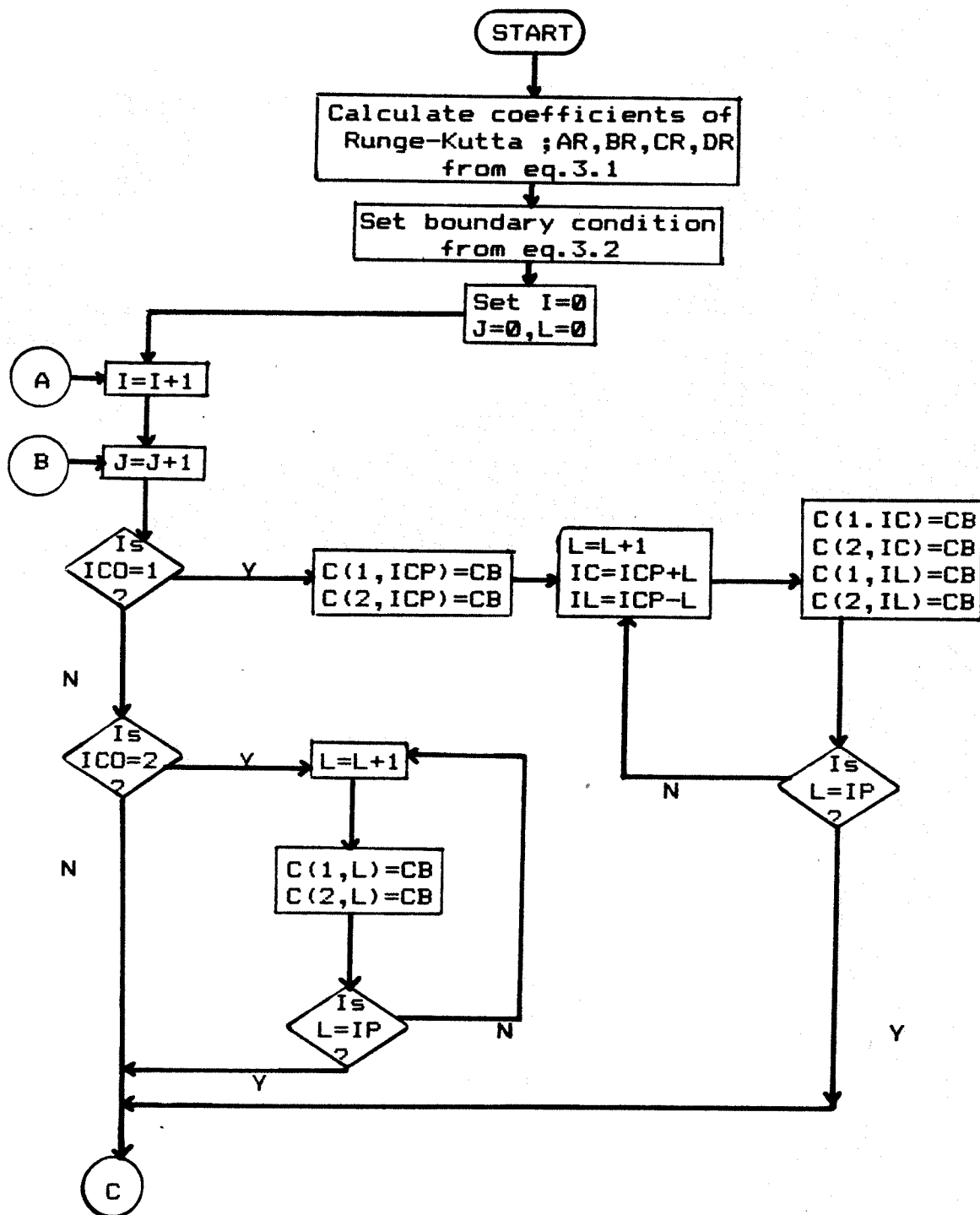
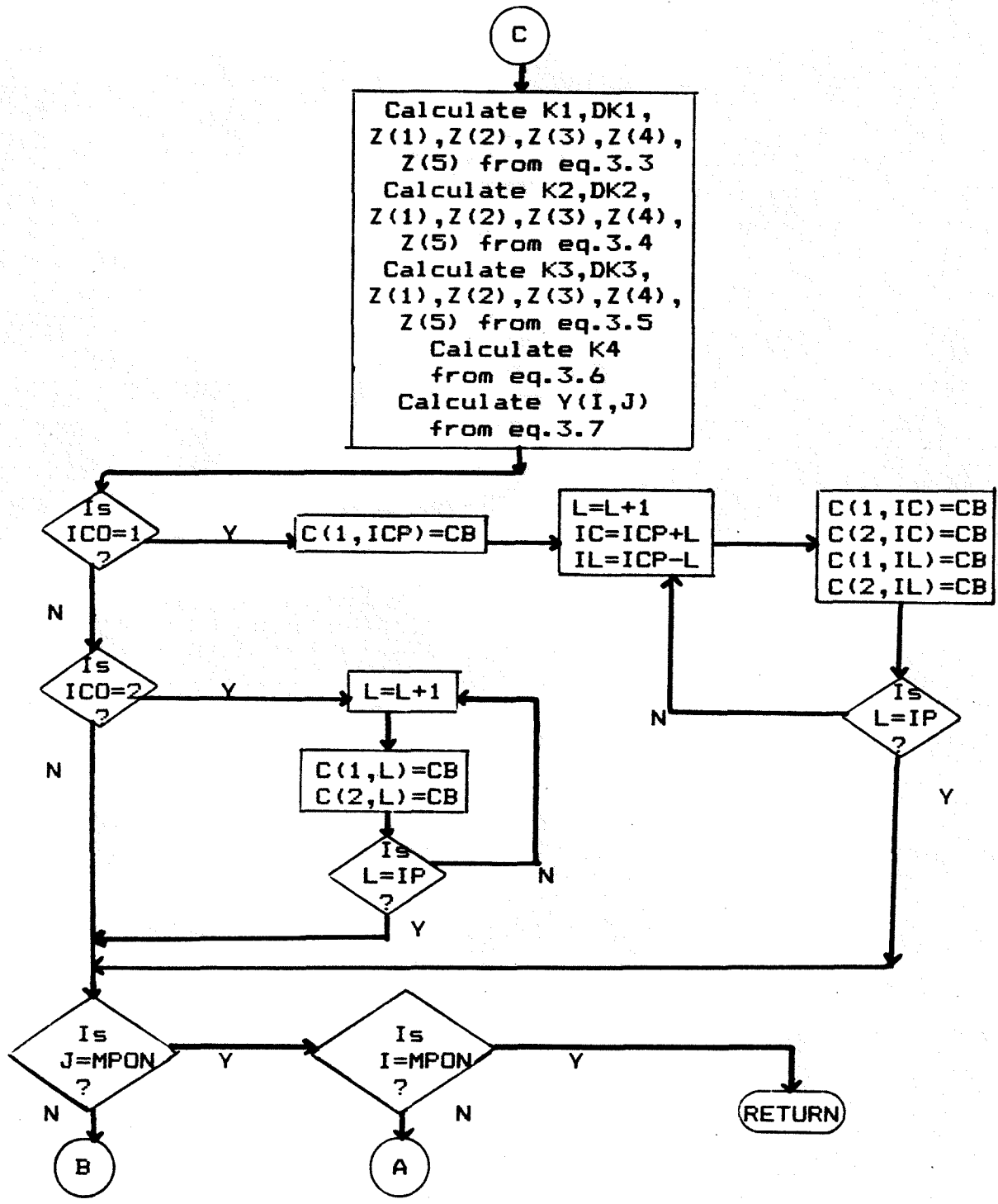


Fig. 3b. Continue flow-diagram of the subroutine "RUNGE".



The Equations Used in Subroutine "RUNGE"

$$\begin{aligned}
 AR &= 1 - 1/(\text{SQRT}(2)) \\
 BR &= 1 + 1/(\text{SQRT}(2)) \\
 CR &= -0.5 + 1/(\text{SQRT}(2)) \\
 DR &= -1/(\text{SQRT}(2))
 \end{aligned}
 \tag{3.1}$$

$$\begin{aligned}
 C(\text{MPON}+1, J) &= C(\text{MPON}, J) \\
 C(I, \text{MPON}+1) &= C(I, \text{MPON})
 \end{aligned}
 \tag{3.2}$$

$$\begin{aligned}
 K1 &= A(1)*(C(I-1, J)+C(I+1, J))+A(5)*C(I, J)+A(3) \\
 &\quad *(C(I, J-1)+C(I, J+1))+B(1)*(C(I, J)-C(I+1, J))+B(2) \\
 &\quad *(C(I, J-1)-C(I, J+1))+B(3) \\
 DK1 &= (DT*K1)/2 \\
 Z(1) &= C(I-1, J) + DK1 \\
 Z(2) &= C(I+1, J) + DK1 \\
 Z(3) &= C(I, J) + DK1 \\
 Z(4) &= C(I, J-1) + DK1 \\
 Z(5) &= C(I, J+1) + DK1
 \end{aligned}
 \tag{3.3}$$

$$\begin{aligned}
 K2 &= A(1)*(Z(1)+Z(2))+A(5)*Z(3)+A(3)*(Z(4)+Z(5))+ \\
 &\quad B(1)*(Z(3)-Z(2))+B(2)*(Z(3)-Z(5))+B(3) \\
 DK2 &= DT*(CR*K1+AR*K2) \\
 Z(1) &= C(I-1, J) + DK2 \\
 Z(2) &= C(I+1, J) + DK2 \\
 Z(3) &= C(I, J) + DK2 \\
 Z(4) &= C(I, J-1) + DK2 \\
 Z(5) &= C(I, J+1) + DK2
 \end{aligned}
 \tag{3.4}$$

$$K3 = A(1)*(Z(1)+Z(2))+A(5)*Z(3)+A(5)*(Z(4)+Z(5))+ \\ B(1)*(Z(3)-Z(2))+B(2)*(Z(3)-Z(5))+B(3)$$

$$DK3 = DT*(DR*K2+BR*K3)$$

$$Z(1) = C(I-1,J) + DK3$$

$$Z(2) = C(I+1,J) + DK3$$

$$Z(3) = C(I,J) + DK3$$

$$Z(4) = C(I,J-1) + DK3$$

$$Z(5) = C(I,J+1) + DK3 \quad (3.5)$$

$$K4 = A(1)*(Z(1)+Z(2))+A(5)*Z(3)+A(3)*(Z(4)+Z(5))+ \\ B(1)*(Z(3)-Z(2))+B(2)*(Z(3)-Z(5))+B(3) \quad (3.6)$$

$$Y(I,J) = C(I,J)+(DT/6)*(K1+(2*AR*K2)+(2*BR*K3)+K4) \quad (3.7)$$

Table of Variables Meaning

Variables	Meaning
A(1) to A(5)	The model coefficients calculated from eq.(2.9).
AR,BR,CR,DR	The coefficients of Runge-Kutta eq.(3.1)
B(1) to B(3)	The model coefficients calculated from eq.(2.9).
C(I,J)	The concentration of FITC-dextran at each grid point.
CB	The initial concentration at a leakage point.
CINI	The measured concentration of FITC-Dextran in the plasma phase; input in SCONV .
CONC	The calculated concentration;output of SCONV.
D	The diffusion coefficient.
DT	The time step (h in Runge-Kutta eq.)
DX,DY	The distance between two points on i-,j-axis.
DK1,DK2,DK3,DK4,Z(1) to Z(5)	The parameters used in Runge-Kutta eq.(3.3), (3.4), and (3.5).
ICO	Represent type of theoritical model.
IP	The number of leakage points.

Variables	Meaning
LPT	The time step point for printing output.
LX,LY	The last values of I and J read from gray-level datafile (used in SCONV program).
MPON	The total number of points on I-,J-axis.
NEND	The number of iterations in MAIN .
R	The reaction rate.
VX,VY	Interstitial velocities on I-,J-axis.
Y	Transfer parameters for calculated concentration from subroutine RUNGE.

Fig.30. Flow-diagram of the "COEFF" program.

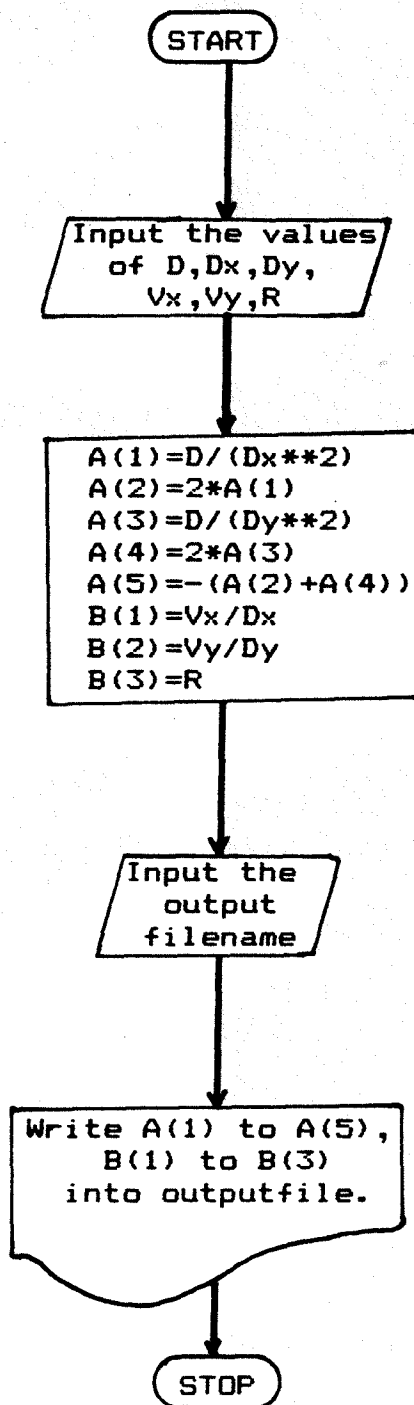


Fig.3d. Flow-diagram of the "BOU" program

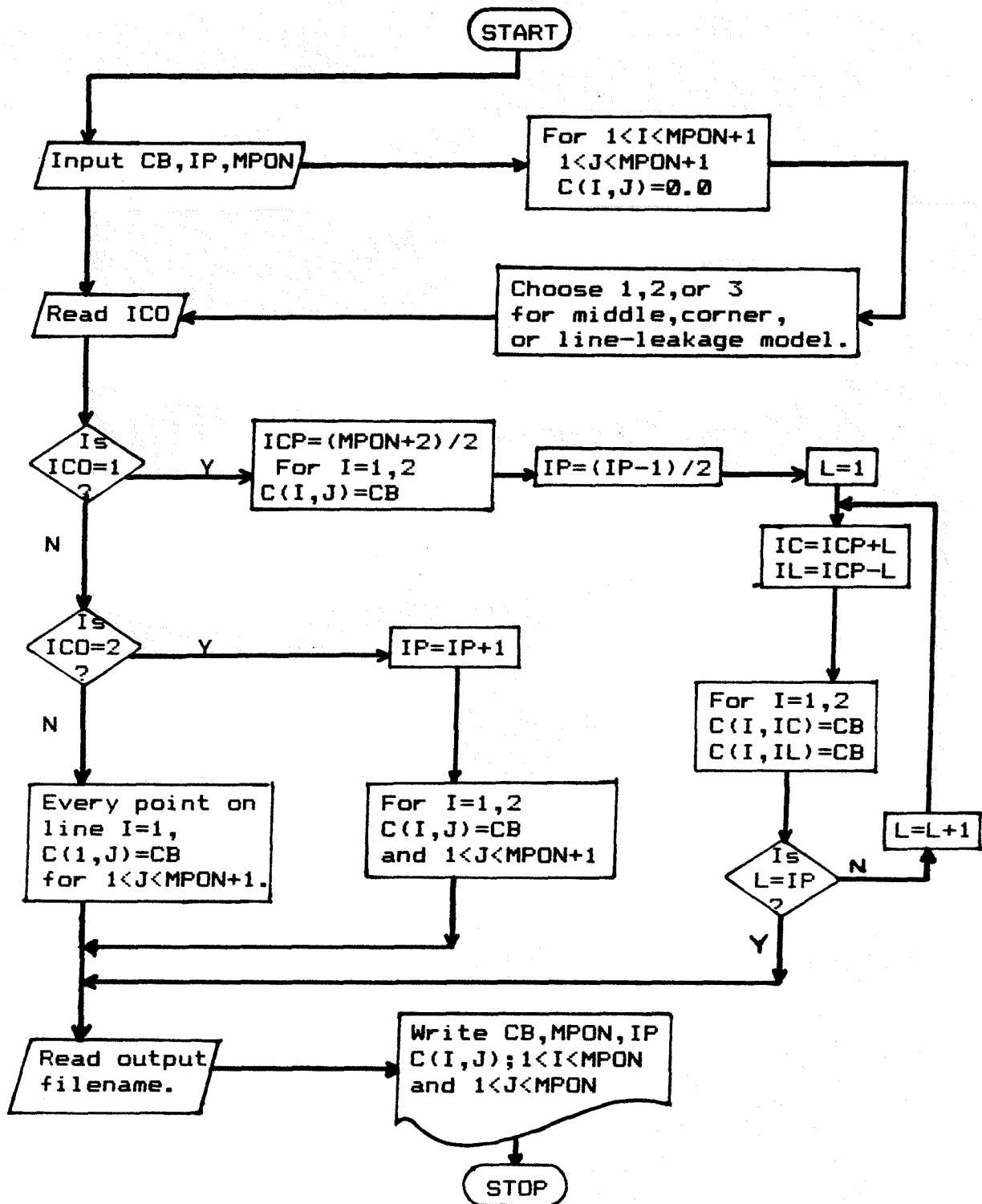
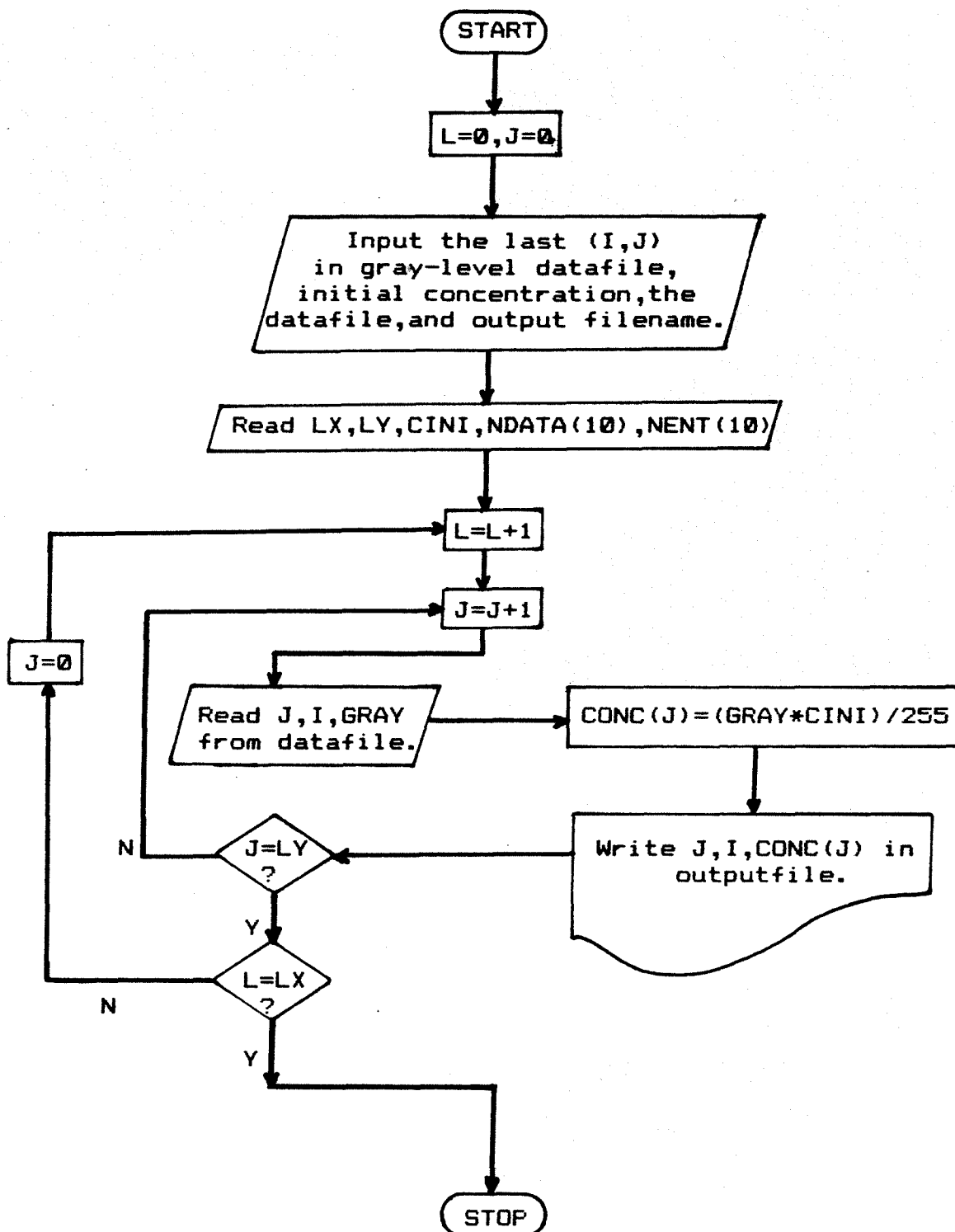


Fig.3e. Flow-diagram of the "SCONV" program, that is used to convert gray level to concentration of FITC-dextran.



The Model Solutions :

There are two major cases which were studied : first, the variation of $C(i,j,t)$ as the position of the leakage points changed; second, the same initial and boundary conditions but the parameters D, V_x , and V_y were varied over a range of values.

1. After the computer model had been set up, three different boundary conditions were evaluated. The three models were :

1.1. MODEL I: A leakage point in the middle of the spatial domain boundary conditions as shown in Fig.3.1. The parameter values used in this simulation were as follows :

$$h = 0.05 \text{ sec} \quad D = 0.01 \text{ um}^2/\text{sec}$$

$$\Delta x = \Delta y = 0.1 \text{ um} \quad V_x = V_y = 0 .$$

This is the case of pure diffusion from a point source with no convection in the interstitial space.

The solution and the theoretical curves are shown in Table 3.1 and in Fig.3.2 .

1.2. MODEL II: A leakage point in the corner of the spatial domain with initial and boundary conditions shown in Fig.3.3 using the same parameters as in model I. The solution and the theoretical curves are shown in Table 3.2 and in Fig.3.4 .

1.3. MODEL III: The boundary condition for this model consisted of the diffusion from leakage points lining the entire y-axis as shown in Fig.3.5. The same parameters as were used in the first and second models, generated the solution in Table 3.3 and the corresponding theoretical curves in Fig.3.6.

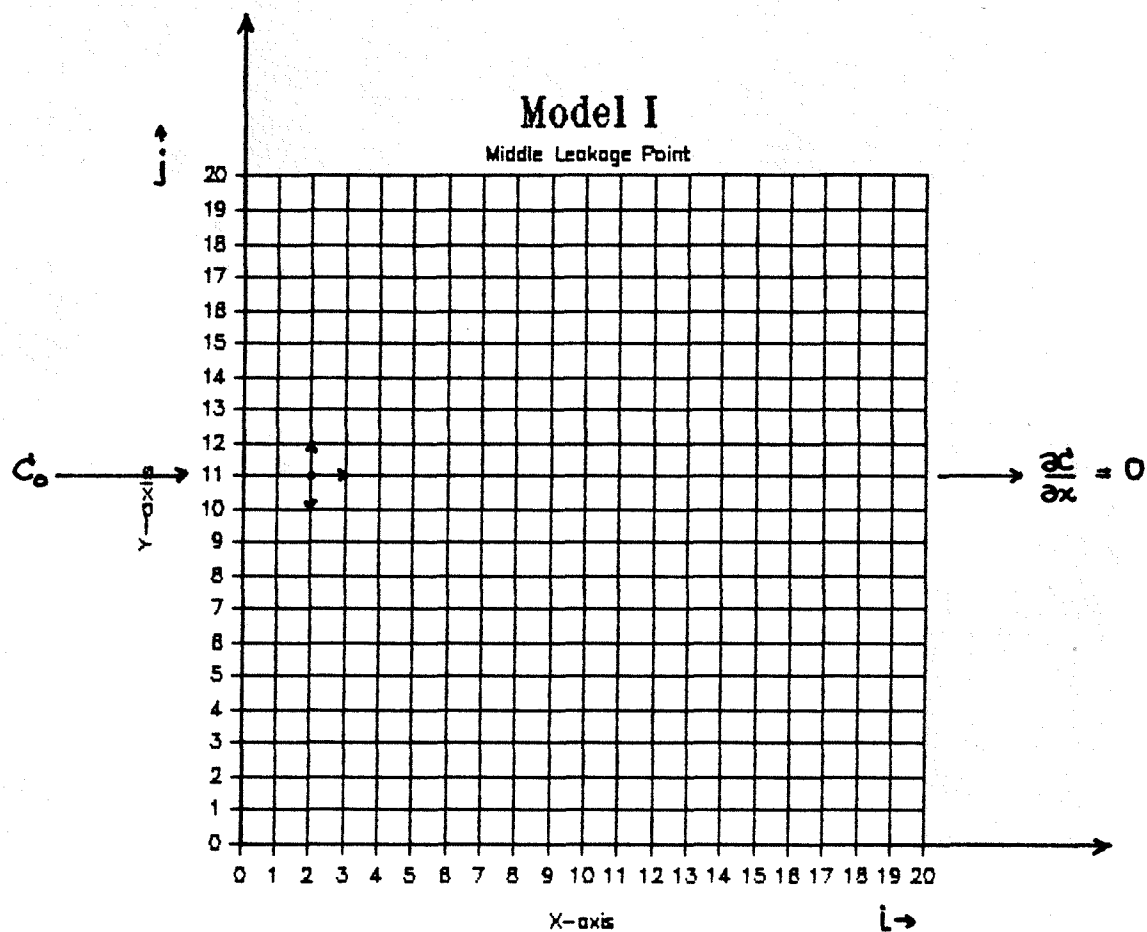


Fig.3.1. The middle-leakage-point model with

initial conditions: $C(1,11,0) = C(2,11,0) = C_0$ (0.86mg/ml)

$C(i,j,0) = 0$; for $3 \leq i \leq 20$, $3 \leq j \leq 20$

boundary conditions : $C(1,j,0) = 0$, $C(2,j,0) = 0$,
for $1 \leq j \leq 20$; except $j=11$

at anytime t : $\frac{\partial C(i,j,t)}{\partial x} = 0$, for $i > 20$
 $\frac{\partial C(i,j,t)}{\partial y} = 0$, for $j > 20$.

TABLE 3.1

A summary of the simulation results for the middle leakage point model which were used to plot the graph in Fig.3.2 .

Distance (um)	Concentration (mg/ml)			
	1.0sec	2.0sec	3.0sec	4.0sec
0.0	0.86	0.86	0.86	0.86
10.0	0.42	0.53	0.59	0.63
20.0	0.15	0.28	0.36	0.42
30.0	0.04	0.05	0.09	0.25
40.0	0.01	0.05	0.09	0.14
50.0	0.00	0.01	0.04	0.07

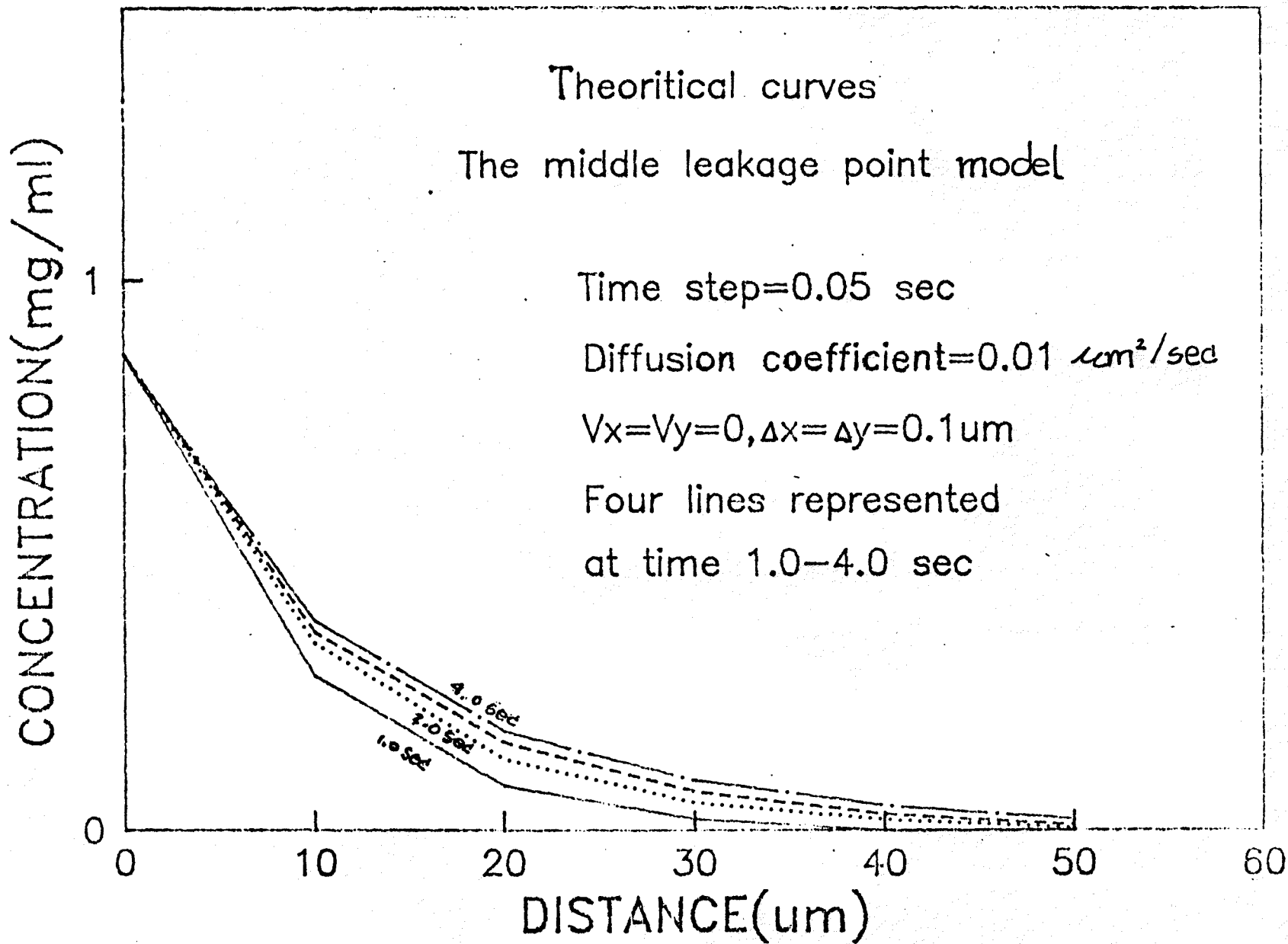


Fig. 3.2.

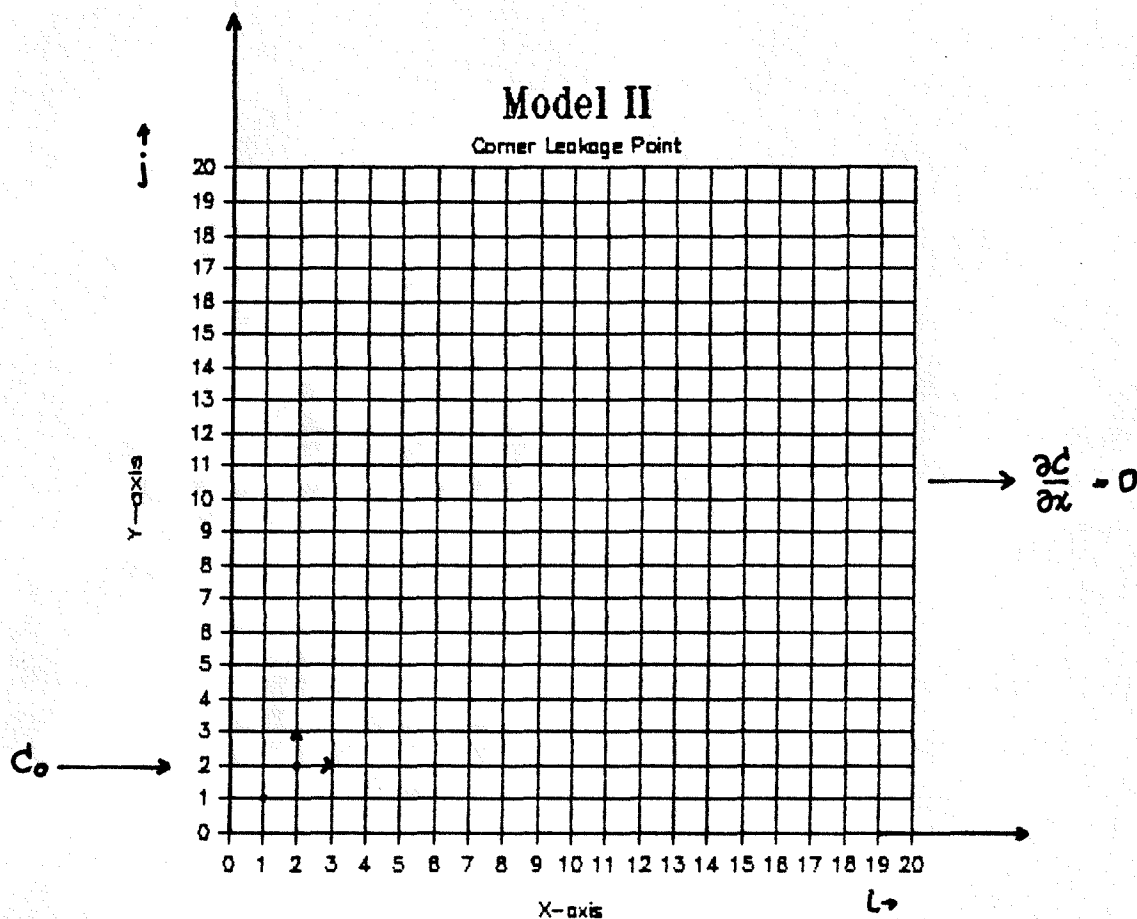


Fig.3.3. The corner-leakage-point model with
 initial conditions : $C(1,1,0) = C(2,2,0) = C_0$ (0.86mg/ml)
 $C(i,j,0) = 0$, for $1 \leq i \leq 20, 1 \leq j \leq 20$
 (except $i=j=1,2$)
 boundary conditions : $\frac{\partial C(i,j,t)}{\partial x} = 0$, for $i > 20$
 at any time t $\frac{\partial C(i,j,t)}{\partial y} = 0$, for $j > 20$.

TABLE 3.2

A summary of the simulation results for the corner leakage point model which were used to plot the graph in Fig.3.4.

Distance (μm)	Concentration (mg/ml)			
	1.0sec	2.0sec	3.0sec*	4.0sec
0.0	0.29	0.30	0.30	0.30
10.0	0.20	0.21	0.21	0.21
20.0	0.11	0.12	0.12	0.12
30.0	0.05	0.07	0.07	0.07
40.0	0.02	0.04	0.04	0.04
50.0	0.01	0.02	0.02	0.03

* This column was not used in plotting the graph, since at 4 sec the concentration at each point was almost the same as the concentration at 3 sec.

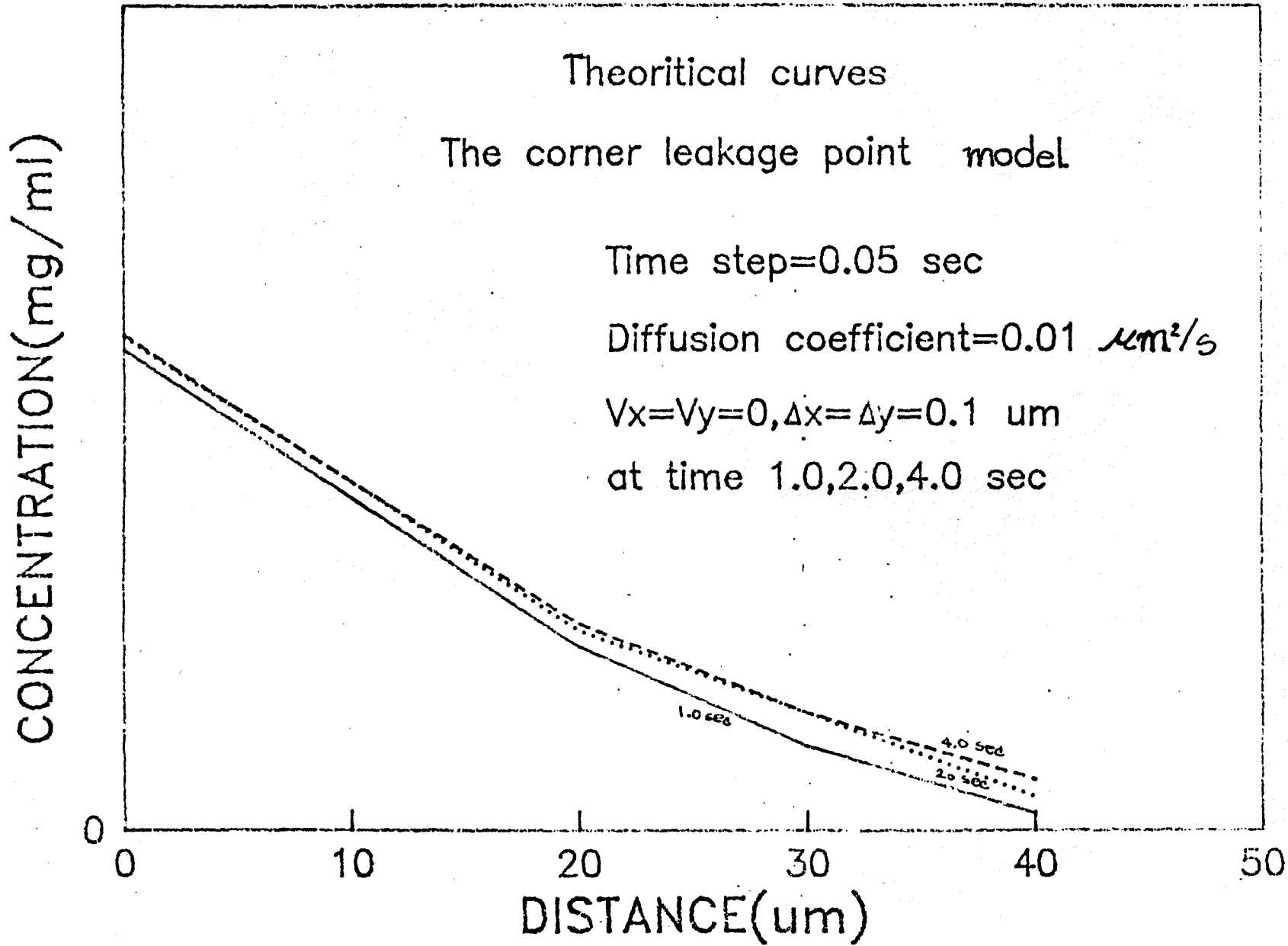


Fig. 3.4.

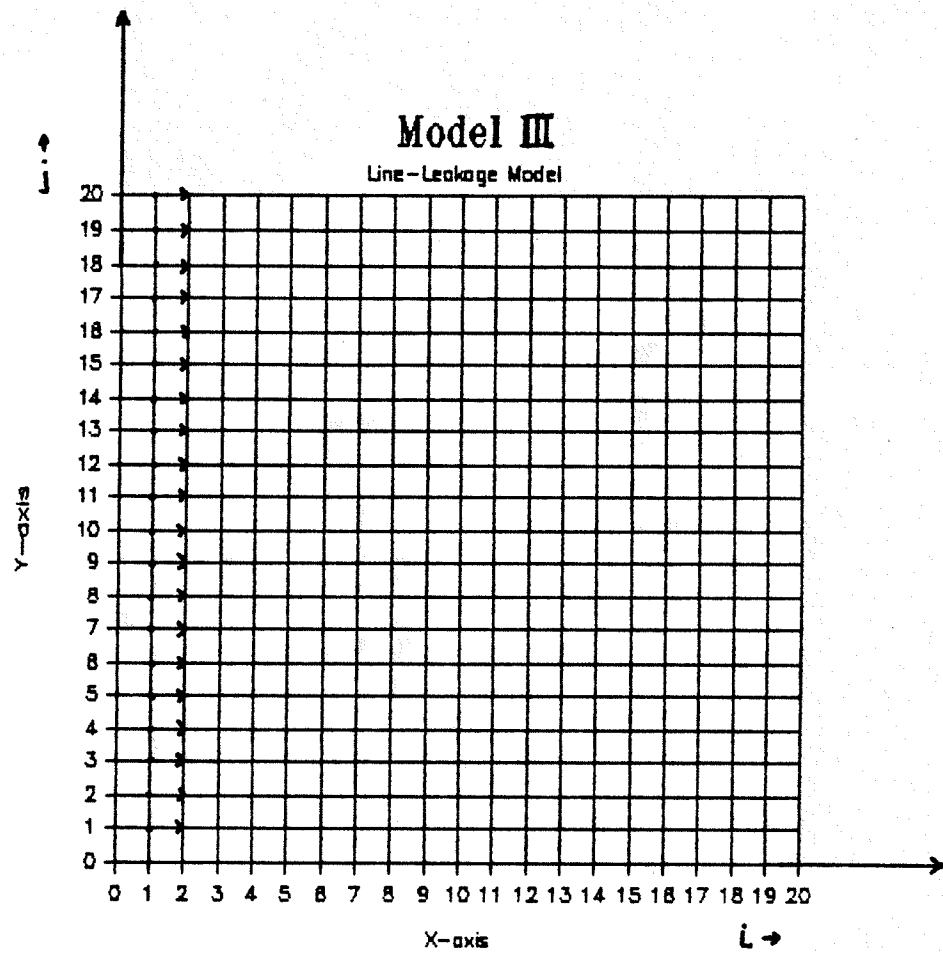


Fig.3.5. The line-leakage model with

initial conditions: $C(1,j,0) = C_0$ (0.86mg/ml) , for $1 \leq j \leq 20$
 $C(i,j,0) = 0$, for $2 \leq i \leq 20$, $2 \leq j \leq 20$

boundary conditions : $\partial C(i,j,t) / \partial x = 0$, for $i > 20$
 $\partial C(i,j,t) / \partial y = 0$, for $j > 20$.

TABLE 3.3

A summary of the simulation results for the line leakage points model which were used to plot the graph in Fig.3.6 .

Distance (um)	Concentration (mg/ml)			
	1.0sec	2.0sec	3.0sec	4.0sec
0.0	0.86	0.86	0.86	0.86
10.0	0.28	0.34	0.36	0.38
20.0	0.08	0.13	0.16	0.18
30.0	0.02	0.05	0.07	0.09
40.0	0.00	0.02	0.03	0.05
50.0	0.00	0.01	0.01	0.02

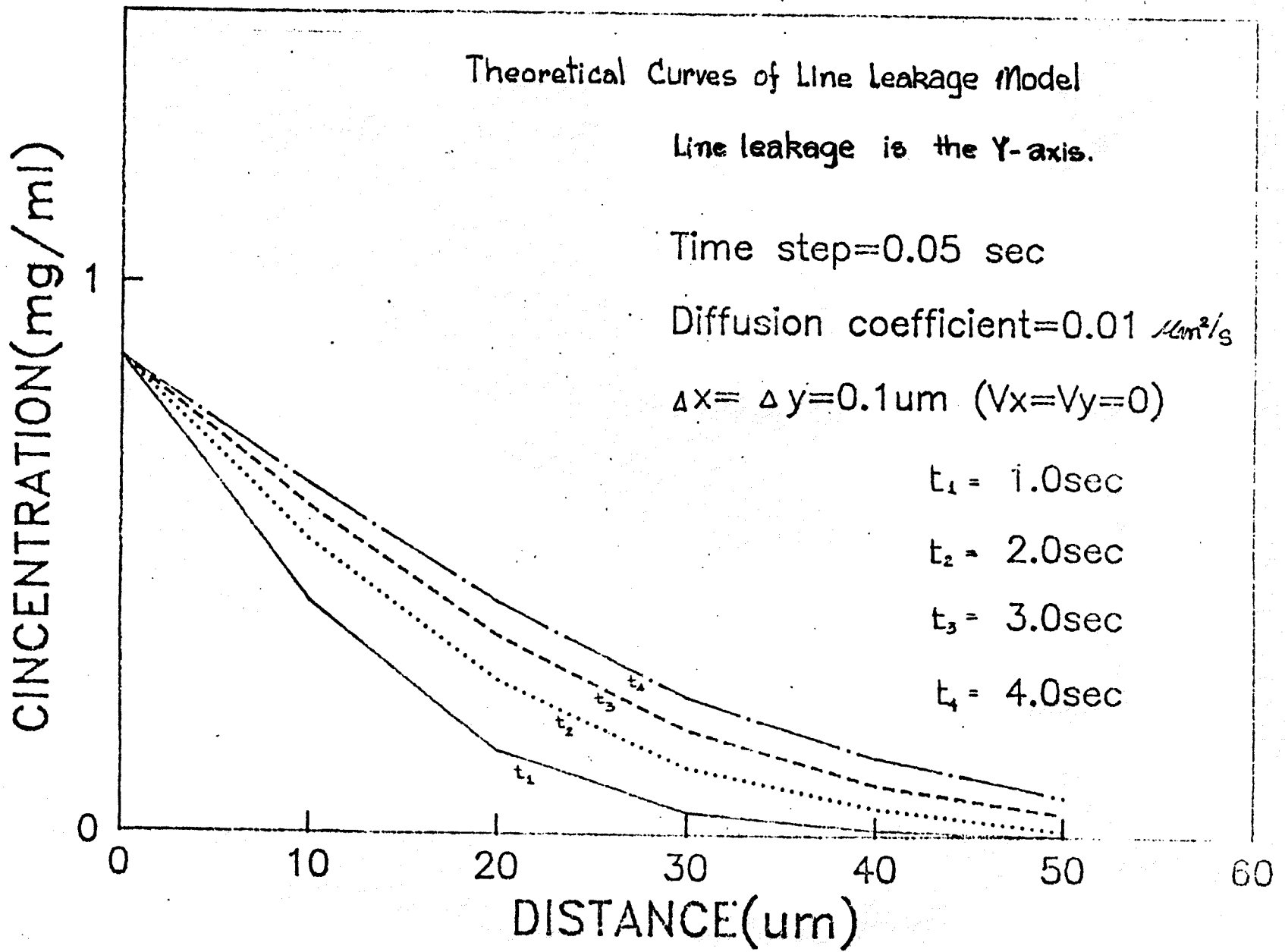


Fig. 3.6

2. The other simulations used nonzero values of V_x and V_y . The differences in the model solutions as indicated by their theoretical curves were as follows :

2.1. Fig.3.7(a,b) ; this shows two solutions for the middle leakage model (the same as in Fig.3.1 except the value of $C_0 = 2.39$ mg/ml). The results show that with $V_x = V_y = 1.0 \times 10^{-4}$ cm/sec, the computed $C(i,j,t)$ is increased at any point at any time by increasing the diffusion coefficient (D).

2.2. The solution is more complex when the model coefficients V_x, V_y are nonzero. When $V_x = V_y = 0$, increasing D increases $C(i,j,t)$. This was not always true when the values of V_x and V_y were not zero. Fig.3.9 shows that increasing V_y decreases $C(i,j,t)$ near the origin.

Increasing both V_x , and V_y when D is kept constant is shown in Fig.3.10(a,b) for the three-leakage point model. Concentration changes along the x-axis is shown for two simulations with different V_x and V_y . In graph (a) the solutions showed concentration differences from the origin point (2,8) to point (14,8). In graph (b) concentration differences were shown from point (2,11) which was not the origin point to point (10,11), so the concentration profiles were different. That means that diffusion along the y-axis had occurred in (b).

It can be concluded that for the same conditions the values of V_x, V_y increased the effective diffusion rate and

increased the diffusion area at the same value of time (if there are no boundary limitations).

Diffusion on X-axis

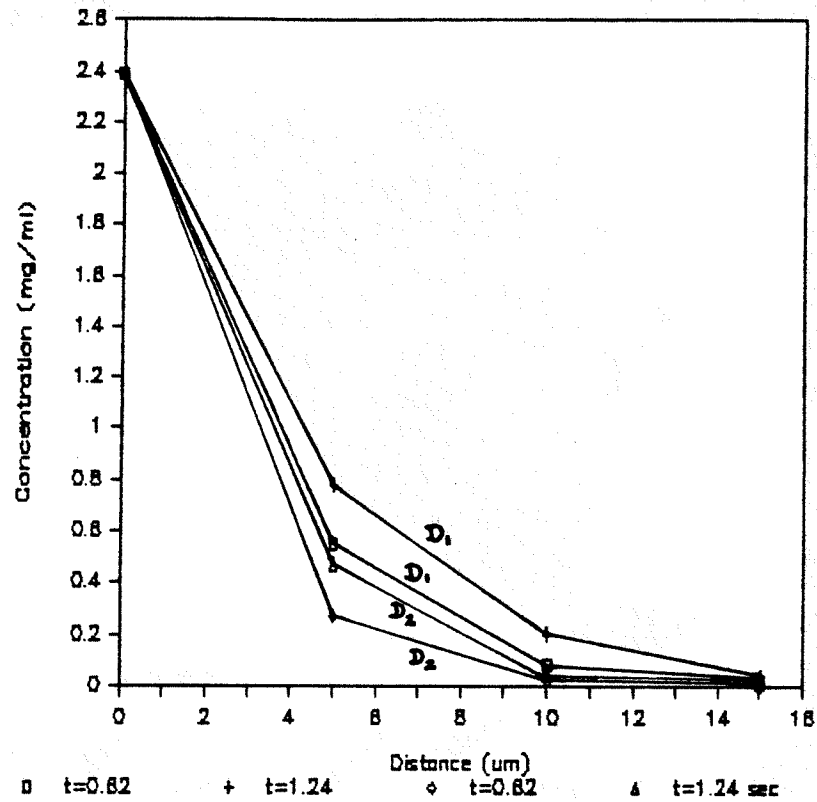


Fig.3.7a. Simulation results for the middle leakage point model (Fig.3.1) with $C_0=2.39$ mg/ml. Two simulations were performed. Both of them used the same values of : $V_x=V_y=1.0 \times 10^{-4}$ cm/sec , $D_x=D_y=5$ um , and $h = 0.062$ sec. The values of D are different as one used $D_1=1.5 \times 10^{-7}$ cm²/sec and the other used $D_2 = 5.0 \times 10^{-8}$ cm²/sec. The concentration profiles along the x-axis at time 0.62 and 1.24 sec are shown for both values of D .

Diffusion on Y-axis

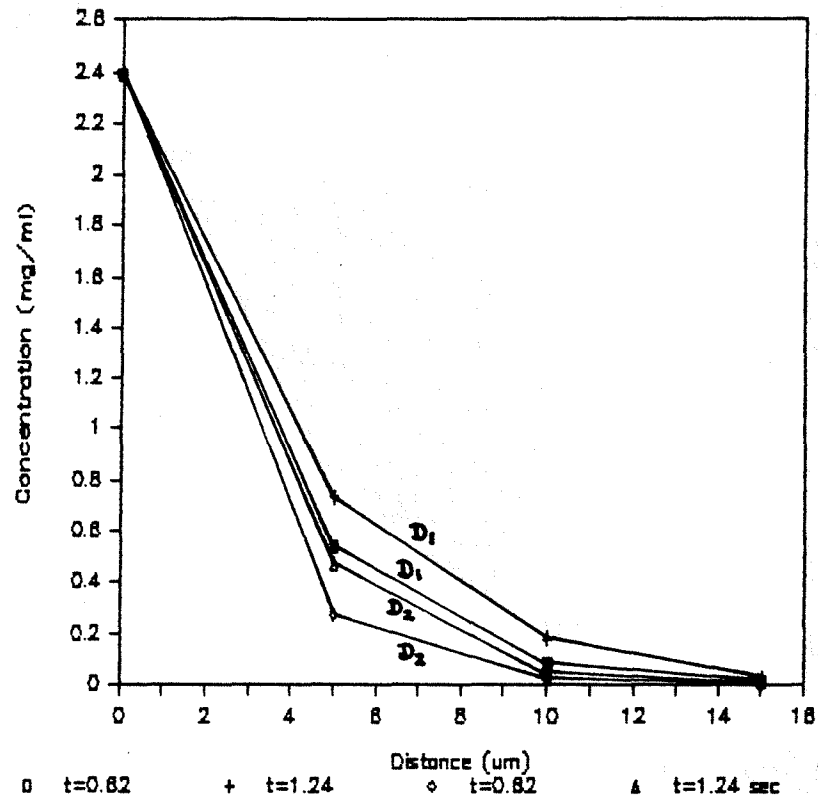


Fig.3.7b. This graph shows the concentration profiles along the y-axis for the simulation shown in Fig.3.7a. With $V_x=V_y=1.0 \times 10^{-4}$ cm/sec and no diffusion heterogeneity, the profiles are identical.

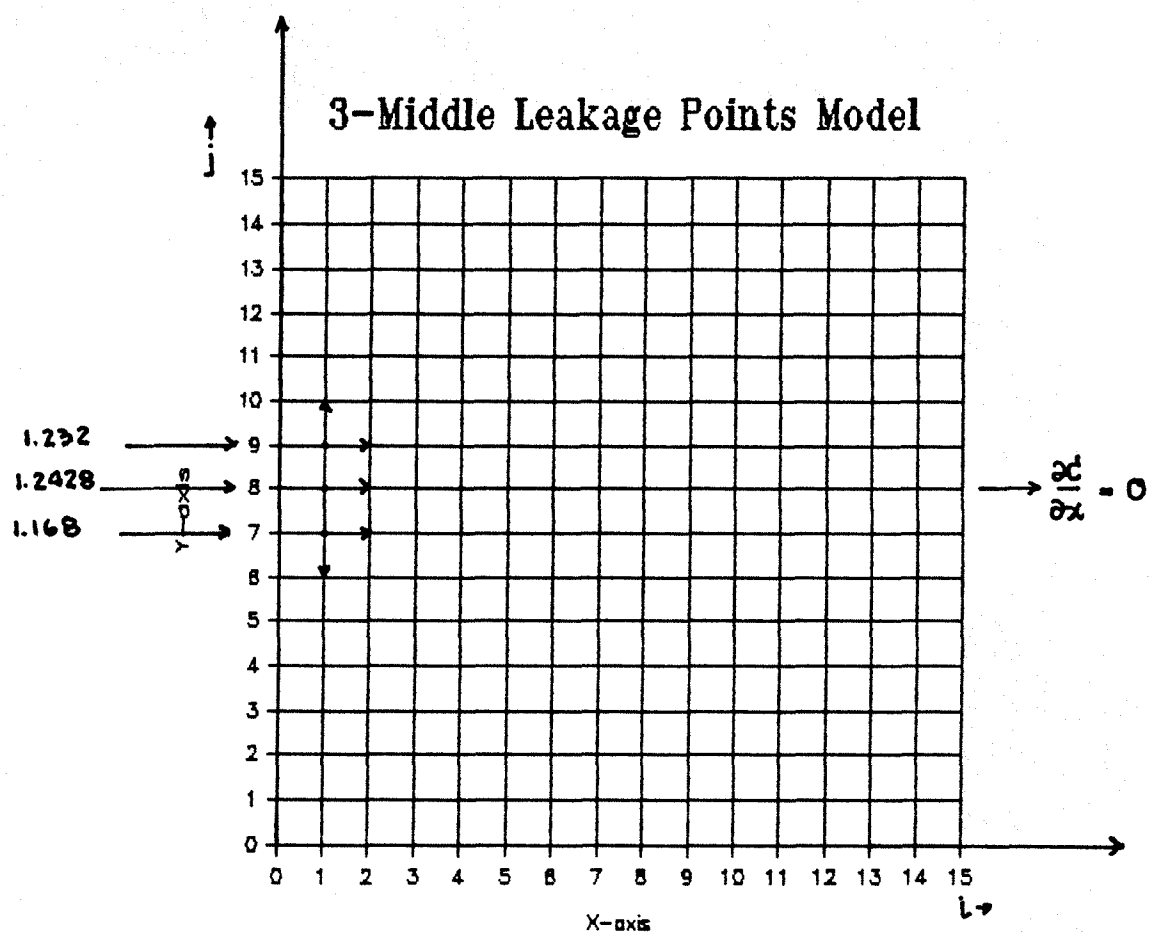


Fig.3.8. Three leakage points model with

initial conditions : $C(0,7,0)=C(1,7,0)=1.168$ mg/ml
 $C(0,8,0)=C(1,8,0)=1.2428$ mg/ml,
 $C(0,9,0)=C(1,9,0)=1.232$ mg/ml
 $C(i,j,0) = 0$; for $2 \leq i \leq 15$, $2 \leq j \leq 15$

boundary conditions : $C(0,j,t) = 0$, for $1 \leq j \leq 15$
 except $C(0,7,t)=1.168$, $C(0,8,t)=1.2428$,
 $C(0,9,t)=1.232$ mg/ml

and

$\frac{\partial C(i,j,t)}{\partial x} = 0$ for $i > 15$
 $\frac{\partial C(i,j,t)}{\partial y} = 0$ for $j > 15$.

Different D Coefficient

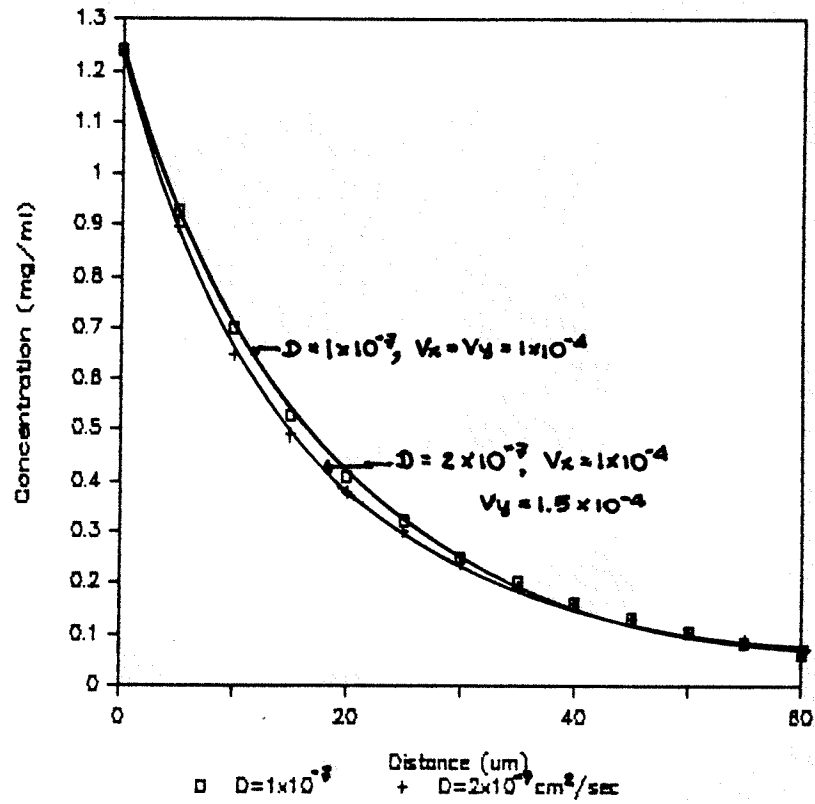


Fig.3.9. Two theoretical curves that calculated using three leakage point model (Fig.3.8) and $D_x=D_y=5 \text{ um}$, $h=0.36 \text{ sec}$. One simulation used $D=1.0 \times 10^{-7} \text{ cm}^2/\text{sec}$, $V_x=V_y=1.0 \times 10^{-4} \text{ cm/sec}$, and the other used $D=2.0 \times 10^{-7} \text{ cm}^2/\text{sec}$, $V_x=1.0 \times 10^{-4}$, $V_y=1.5 \times 10^{-4} \text{ cm/sec}$. Concentration profiles on the x-axis at time 53 sec are shown.

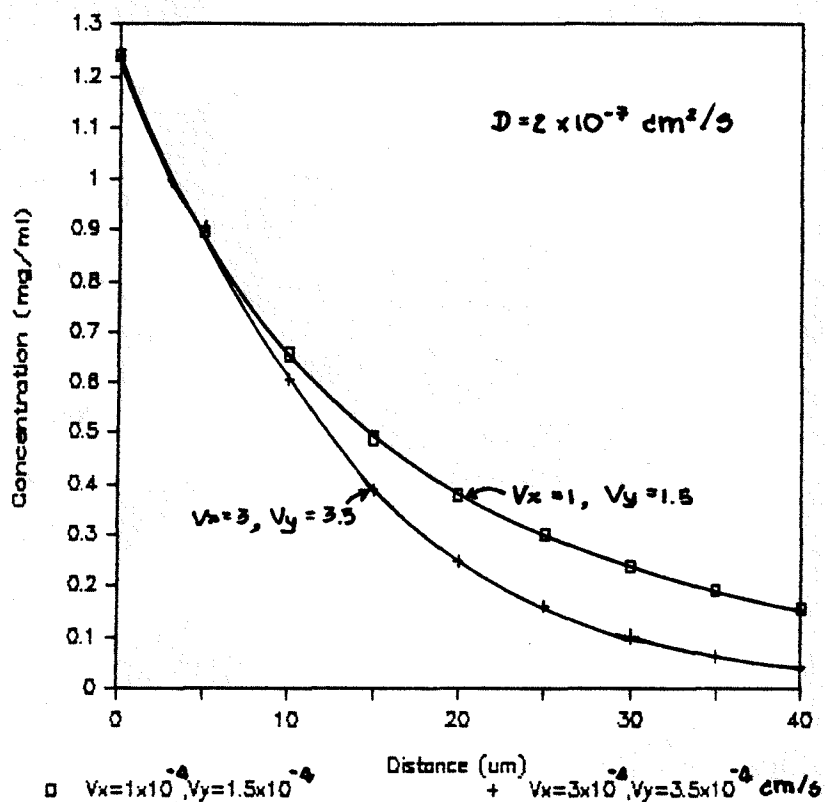
Different V_x, V_y 

Fig.3.10a. Using the three point leakage model as shown in Fig.3.8, one simulation used $V_x = 1 \times 10^{-4}$, $V_y = 1.5 \times 10^{-4}$ cm/sec, and the other used $V_x = 3 \times 10^{-4}$, $V_y = 3.5 \times 10^{-4}$ cm/sec. Both used the same $D = 2.0 \times 10^{-7}$ cm²/sec, $D_x = D_y = 5$ um, and $h = 0.36$. The concentration profile along the x-axis at time 53 sec is shown.

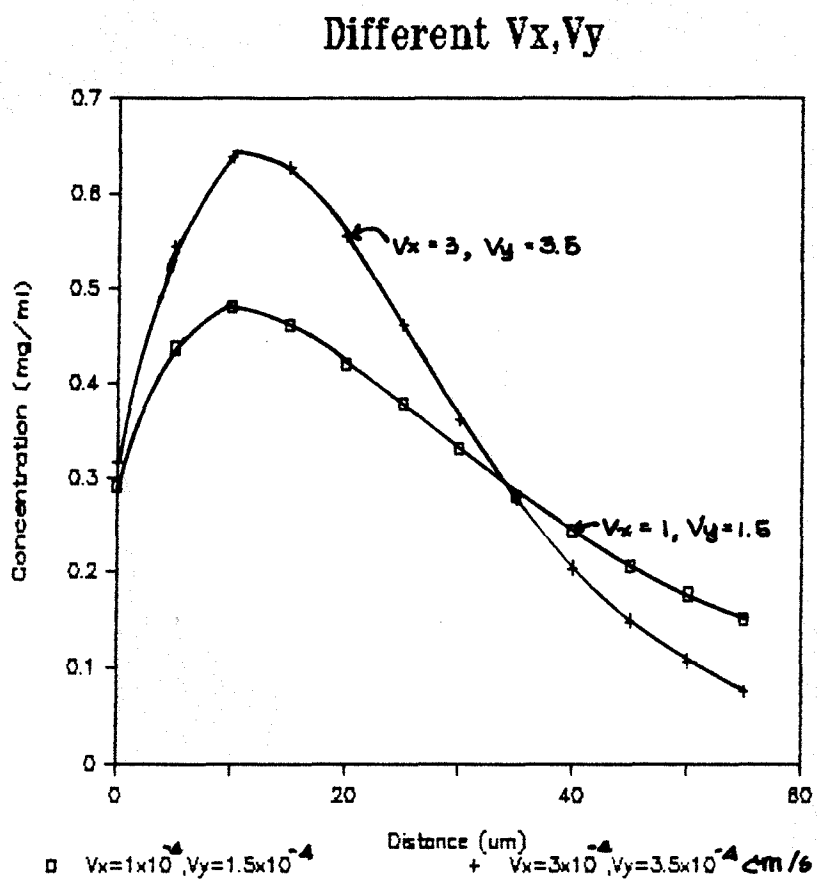


Fig.3.10b. The same simulation as in Fig.3.10(a) is shown but this figure shows the concentration profile from point (2,11) to point (10,11) at time 53 sec.

In these simulations we have to be concerned about the stability of the numerical method so that the solution is valid. As mentioned before; the time step, h , should be selected so that :

$$h(2D/(D_x^2 + D_y^2)) < 1/2 .$$

This relationship has been determined by step-by-step methods for initial value problems (ref.7). The value "1/2" is called the "modulus" of the equation, and was chosen so that all coefficients in eq.(3.1) were positive for a stable solution.

To illustrate the dependence of the stability of the solution on the step size chosen, Table 3.4 shows the results of a simulation in which the parameters were kept constant and h (the time step size) was changed from 0.062 sec to 0.62 sec. Clearly, the results of the second simulation were erratic and not stable. A further simulation with h reduced to 0.01 sec gave results which were barely distinguishable from the first simulation. Thus the time step size required for stability in the step-by-step method appeared to be suitable for the Runge-Kutta method but attempts to use a larger step size in the Runge-Kutta method results in instability.

TABLE 3.4

Distance (um)	The first simulation Concentration(mg/ml)		The second simulation Concentration(mg/ml)	
	6.2sec	1.24sec	6.2sec	1.24sec
0	2.39	2.39	2.39	2.39
5	0.996	1.088	-0.96×10^{11}	-0.144×10^{24}
10	0.447	0.572	0.95×10^{11}	0.19×10^{24}
15	0.182	0.312	-0.53×10^{11}	-0.166×10^{24}
20	0.073	0.17	0.19×10^{11}	0.109×10^{24}

Parameter values :

$$C_o = 2.39 \text{ mg/ml}$$

$$D_1 = D_2 = 1.0 \times 10^{-6} \text{ cm}^2/\text{sec}$$

$$V_{x_1} = V_{y_1} = V_{x_2} = V_{y_2} = 1 \times 10^{-4} \text{ cm/sec}$$

$$Dx_1 = Dy_1 = Dx_2 = Dy_2 = 5 \text{ um}$$

$$h_1 = 0.062 \text{ sec:}$$

$$D_1(1/Dx_1^2 + 1/Dy_1^2) h_1 = (100 \times 2/25) \times 0.062 = 0.496 < 1/2$$

$$h_2 = 0.62 \text{ sec:}$$

$$D_2(1/Dx_2^2 + 1/Dy_2^2) h_2 = (100 \times 2/25) \times 0.62 = 4.96 > 1/2$$

RESULTS

A Comparison between Experimental Data and Solutions of The Mathematical Models :

Data From The First Experiment

After plotting the experimental concentration profiles as shown in Fig.1.1 and 1.2, two subregions were chosen from Fig.1.1 to compare with the model simulations.

From the plot of the experimental leakage data and from knowing the gray level of each pixel during the control (no leakage) period, the leaking subregion can be determined as shown in Fig.4.1. From the point (45,53) to point (60,53), the concentration profile along the x-axis should be better for comparing than the profile along the y-axis since the tranvascular movement of fluorescently labeled dextran occurred in that area (indicated by small arrows in Fig.4.1). The second subregion was chosen to study the diffusion along the y-axis. Again, by knowing the gray level during the control (no leakage) period, with the data of Fig.1.1, the other subregion from point (42,45) to point (42,31) was chosen (Fig.4.2).

These two subregions were used for comparison with the model as shown in Fig.4.1 and 4.2, since their initial and boundary conditions are approximately the same as those of at a model with four-leakage points and 15x15 arrays of picture elements (Fig.4.3).

Table 4.1 and 4.2 show the corrected gray level differences* and the calculated concentration distribution of FITC-Dextran in subregions studied.

The distance between two pixels in Fig.1.1 is approximately 3 μm . This was determined by calibration using a micrometer scale on the microscope stage at the same magnification which was used in the experiment.

In Fig.4.4 the square dots and the circular dots represent the concentration data in Table 4.1 and 4.2 plotted against the distance between two pixels (3 μm) and the solid lines are the solutions of the best fit theoretical model (Table 4.3) calculated by eq.(3.2) with apparent diffusion coefficient $D' = 1.0 \times 10^{-7} \text{ cm}^2/\text{sec}$ and equal interstitial velocities $V_x, V_y = 1.0 \times 10^{-4} \text{ cm}/\text{sec}$.

* The initial condition for the theoretical model is that $C(x,y,0)=0$. Therefore, the mean values gray level at each x,y point for the control period had to be found before subtraction processing.

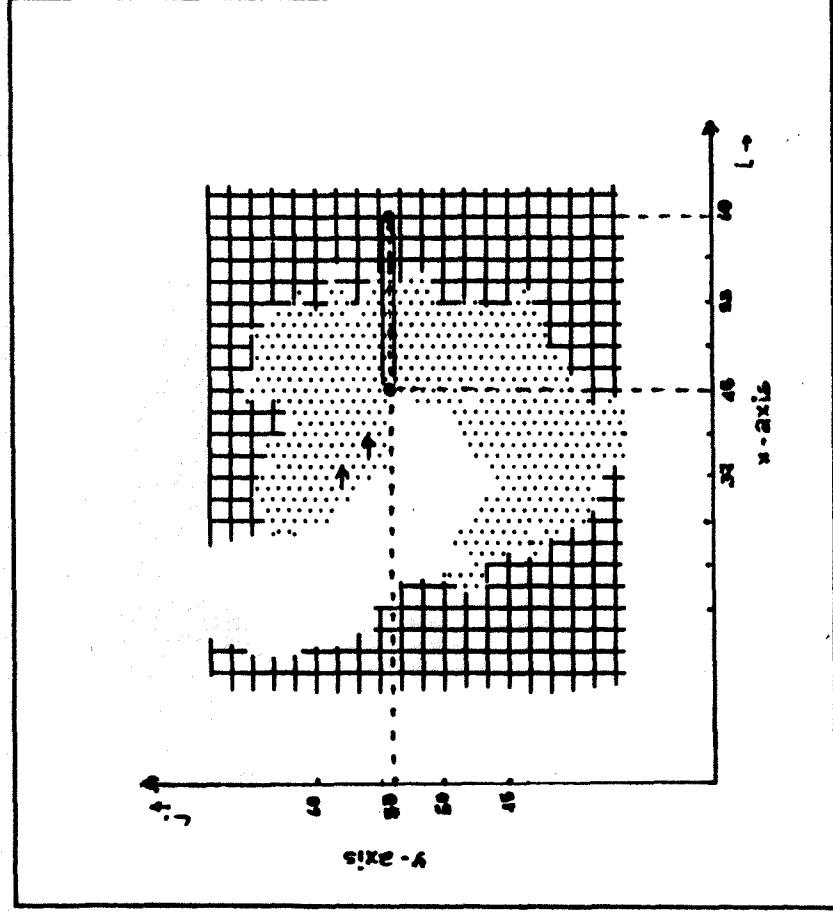


Fig.4. 1. The first subregion selected from Fig.1.1, the gray-level difference from point (45,53) to (60,53) are converted to concentration of FITC-dextran and then plotted against distance along the y-axis in Fig.4. 4.

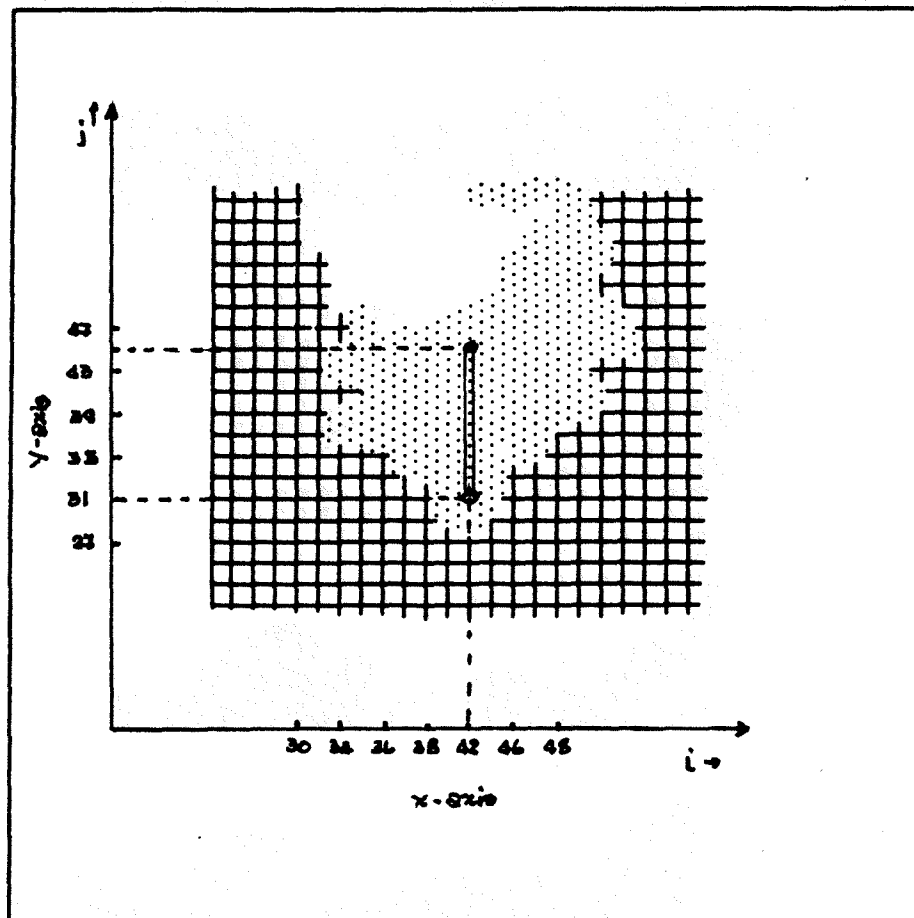


Fig.4.2. The second subregion selected from Fig.1.1. The graylevels converted to concentration from points (42,45) to (42,31) are plotted vs. distance on the y-axis in Fig.4.4.

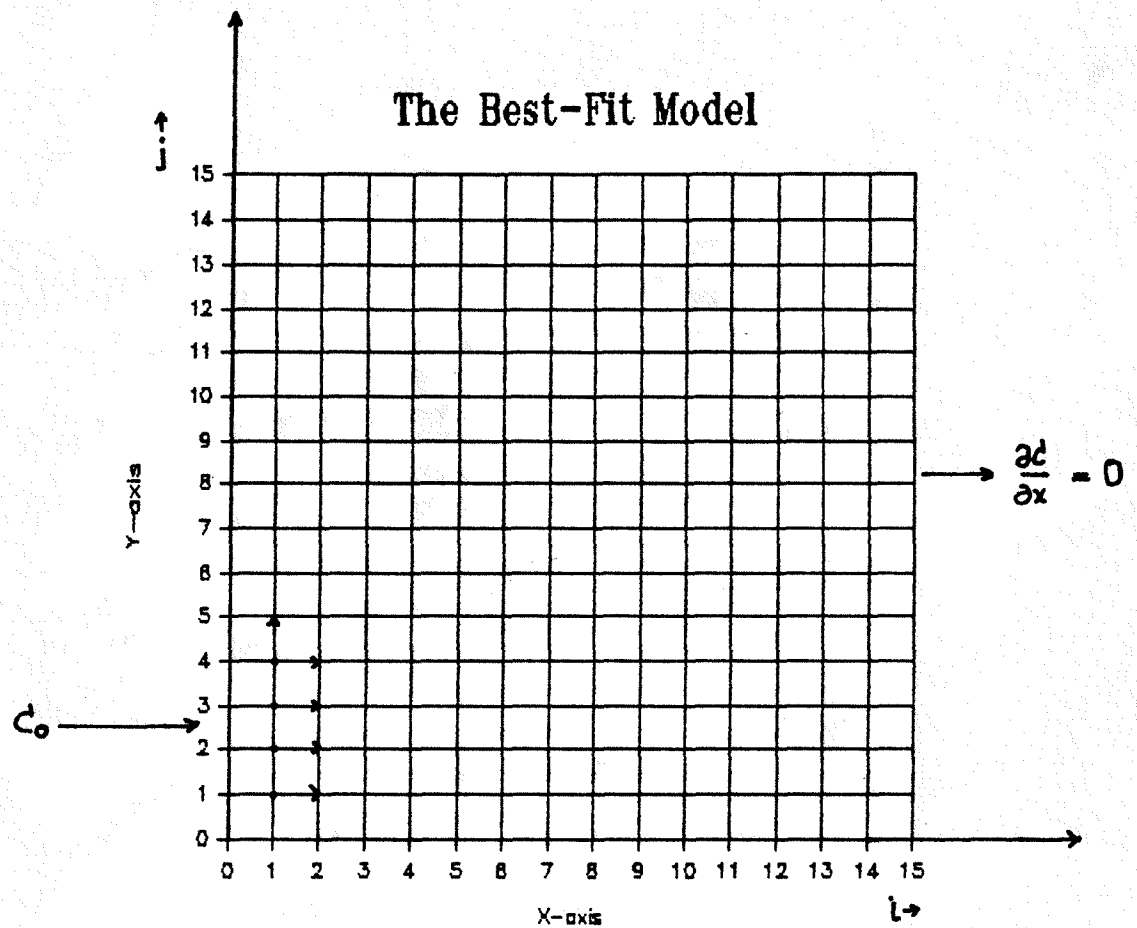


Fig.4.3. The four-leakage-point model. This model gave the best fit of the first set of experimental data, with initial conditions: $C(1,1,0)=C(1,2,0)=C(1,3,0)=C(1,4,0) = C_0 = 1.36 \text{ mg/ml}$, and $C(i,j,0) = 0$, for $2 \leq i \leq 15, 2 \leq j \leq 15$ and boundary conditions: $C(0,j,t) = C_0$, for $1 \leq j \leq 4$,
 $C(0,j,t) = 0$, for $j > 4$
 at any time t : $\partial C(i,j,t)/\partial x = 0$, for $i > 15$,
 $\partial C(i,j,t)/\partial y = 0$, for $j > 15$

TABLE 4.1.

The position, gray level, and calculated concentration at each pixel (selected from Fig.1.1) which was used for the graph in Fig.4.4.

Y	X	Corrected gray level	Concentration* (mg/ml)	Distance along x-axis (um)
53	45	64	0.60	0.0
53	46	55	0.52	3.0
53	47	51	0.48	6.0
53	48	48	0.45	9.0
53	49	43	0.40	12.0
53	50	41	0.38	15.0
53	51	40	0.37	18.0
53	52	38	0.36	21.0
53	53	30	0.28	24.0
53	54	30	0.28	27.0
53	55	25	0.23	30.0
53	56	21	0.20	33.0
53	57	17	0.16	36.0

* Concentration = (gray levelx2.39)/ 255 mg/ml.

TABLE 4.2.

The position, gray level, calculated concentration at each pixel (selected from Fig.1.1) used in Fig.4.4.

X	Y	Corrected gray level	Concentration* (mg/ml)	Distance along y-axis (um)
42	41	53	0.50	0.0
42	40	53	0.50	3.0
42	39	44	0.41	6.0
42	38	44	0.41	9.0
42	37	37	0.35	12.0
42	36	39	0.36	15.0
42	35	38	0.36	18.0
42	34	32	0.30	21.0
42	33	28	0.26	24.0
42	32	28	0.26	27.0
42	31	30	0.28	30.0

* Concentration = (gray levelx2.39)/ 255 mg/ml.

TABLE 4.3.

The solution of the theoretical model for 53-sec
diffusing time; used in Fig.4.4.

Distance (μm)	X-AXIS Concentration* (mg/ml)	Y-AXIS Concentration* (mg/ml)
0.0	0.58	0.48
4.0	0.54	0.48
8.0	0.48	0.46
12.0	0.42	0.42
16.0	0.36	0.37
20.0	0.31	0.33
24.0	0.26	0.28
28.0	0.22	0.24
32.0	0.18	0.20
36.0	0.15	0.18
40.0	0.13	0.16
44.0	0.11	

* Calculated using the following parameters :
time step = 0.20, at 265 iterations = $0.2 \times 265 = 53\text{sec.}$
initial concentration = $(145 \times 2.39) / 255 = 1.36 \text{ mg/ml}$
diffusion coefficient = $10.0 \text{ } \mu\text{m}^2/\text{sec}$
interstitial velocity = $1.0 \text{ } \mu\text{m}/\text{sec}, \Delta x = \Delta y = 4.0 \mu\text{m}$

Comparison of 4 Leakage Point Model with Data of 8/25/80.

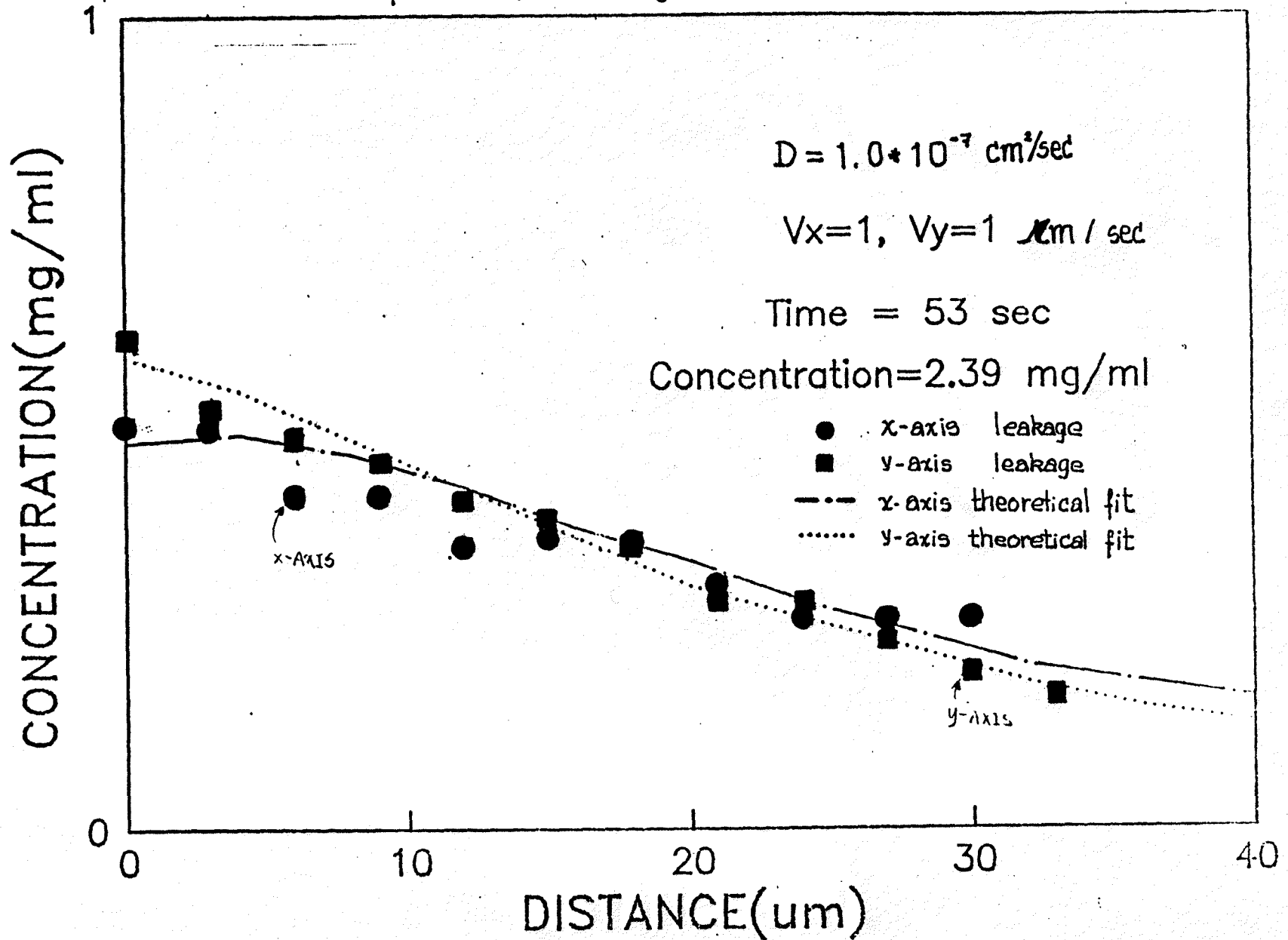


Fig. 4.4.

Data From The Second Experiment

The graph in Fig.1.3 shows the FITC-dextran leakage pattern around a postcapillary venule leakage site in the hamster cheek pouch 31 sec after leakage began. Leakage was induced by topical application of 10^{-5} M Bradykinin for 5 min. The Bradykinin was removed and a continuous stream of buffer bathed the preparation during the leakage time. The control period graylevels were first subtracted leaving only the graylevel differences in grayscale (concentration) between Bradykinin application and control period.

Figure.4.5a shows the position of the leaking vessel. Since the vessel was positioned along a diagonal, the x and y axes were chosen as parallel to and perpendicular to the vessel. The lengths along the axes had to be calculated from the pixel dimensions and the graphscale values along the x and y axes were taken as the values of gray level in those pixels on the opposite corner of each little square (Fig.4.5a,4.5b). The length calculation is illustrated in Fig.4.5b.

Fig.(4.6a,4.6b) shows the concentration profiles along the x and y axes (Table 4.4) in this subregion. The dotted lines represent the solution of the three-leakage point model for the parameter values given in Table 4.5.

The other subregion was chosen around a second leakage site (Fig.4.7) and the concentration at each x,y point after 31-sec diffusion (Table 4.6, Fig.4.8) was also fit by the same model(Fig.4.3, except $C_0=2.39$ mg/ml) using the same parameter values as were used to fit the data at the first subregion. This serves as a check on the parameter estimated from the model.

The result of the simulation of the second experiment gave the estimated interstitial diffusion coefficient and interstitial velocities for FITC-dextran ($\bar{M}_w = 150,000$) as :

$$D' = 1.0 \times 10^{-7} \text{ cm}^2/\text{sec}$$
$$V_x = V_y = 1.0 \times 10^{-4} \text{ cm/sec.}$$

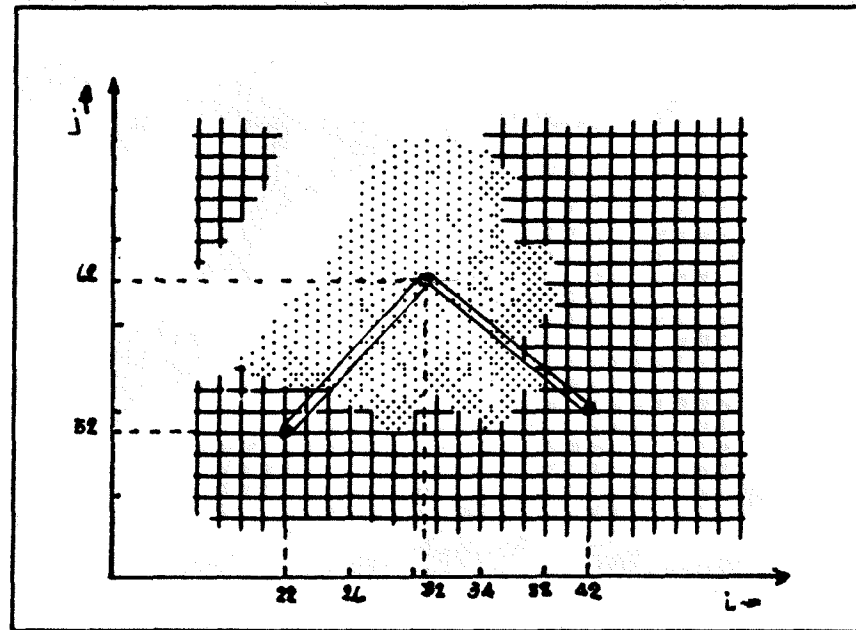


Fig.4.5a. The first subregion selected from Fig.1.3, calculated concentrations at points (32,62) to (22,52) and at points (32,62) to (42,52) were used in the plot against distance on the y-axis and the x-axis, respectively, in Fig.4.6(a,b).

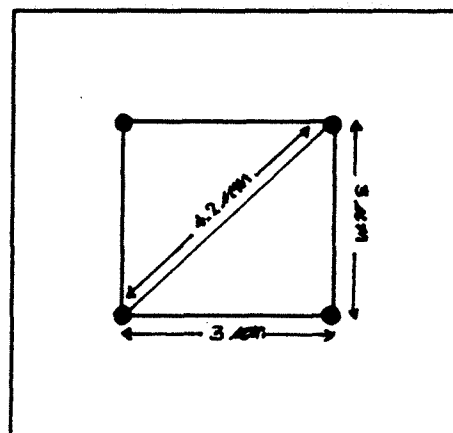


Fig.4.5b. The distance between each pixel used in Fig.4.6a, was calculated from the length of a diagonal line through the pixel.

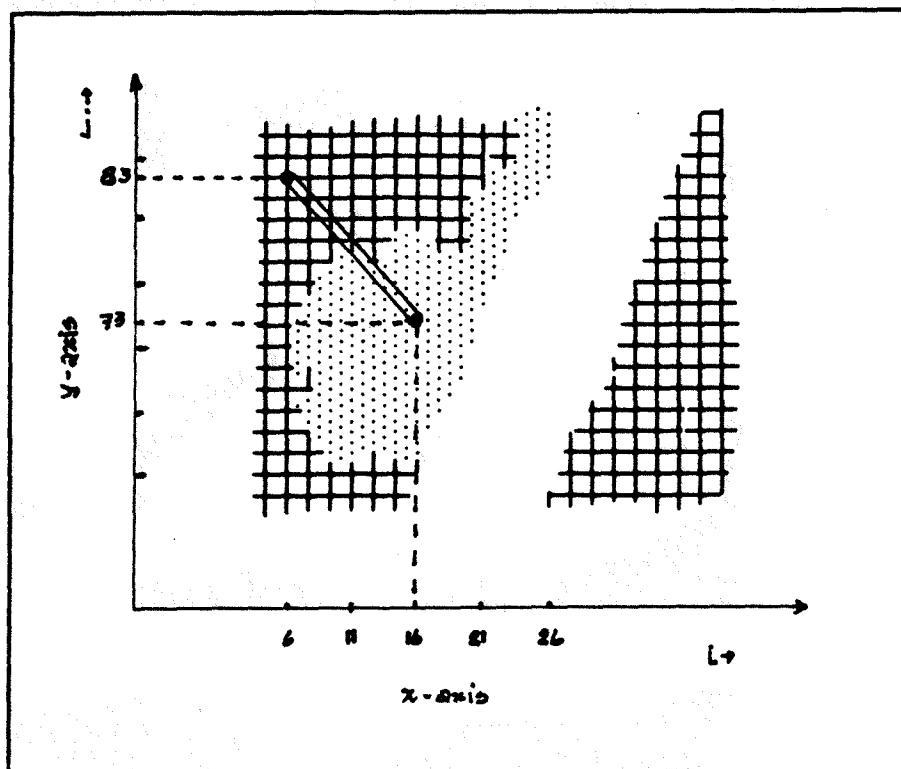


Fig.4.7 The second subregion selected from Fig.1.3, the calculated concentrations at points (16,73) to (6,83) were used to plot the graph in Fig.4.8.

TABLE 4.4.

The position, gray level, calculated concentration at each pixel (selected from Fig.1.3) used in Fig.(4.6a,4.6b).

Y*	X	Y-AXIS Concentration (mg/ml)	X*	Y	X-AXIS Concentration (mg/ml)	Distance (um)
62	32	0.84	32	62	0.84	0.0
61	31	0.81	33	61	0.81	4.0
60	30	0.57	34	60	0.65	8.0
59	29	0.54	35	59	0.53	12.0
58	28	0.53	36	58	0.48	16.0
57	27	0.35	37	57	0.19	20.0
56	26	0.26	38	56	0.29	24.0
55	25	0.24	39	55	0.30	28.0
54	24	0.23	40	54	0.32	32.0
53	23	0.19	41	53	0.21	36.0
52	22	0.13	42	52	0.15	40.0

* Diffusion along the lines perpendicular and parallel to the leaking vessel.

TABLE 4.5.

The solution of theoretical model used for comparison with the 31-sec diffusing time data(Fig.1.3).

Distance (μm)	X-AXIS Concentration* (mg/ml)	Y-AXIS Concentration* (mg/ml)
0.0	0.93	0.93
4.0	0.82	0.82
8.0	0.70	0.70
12.0	0.58	0.58
16.0	0.48	0.47
20.0	0.38	0.37
24.0	0.30	0.29
28.0	0.24	0.23
32.0	0.18	0.18
36.0	0.14	0.15
40.0	0.12	

* Calculated from the theoretical model with the following parameters :
time step = 0.10 sec, at 310 iterations $\Delta t = 0.1 \times 310 = 31 \text{ sec}$
initial concentration = 2.39 mg/ml
diffusion coefficient = 10.0 $\mu\text{m}^2/\text{sec}$
solvent velocity (V_x, V_y) = 1.0 $\mu\text{m}/\text{sec}$, $\Delta x = \Delta y = 4.0 \mu\text{m}$.

** The control gray level distribution for the control period was not available, so it was assumed that the leaking points had the same concentration as was experimentally measured in the plasma phase of the animal.

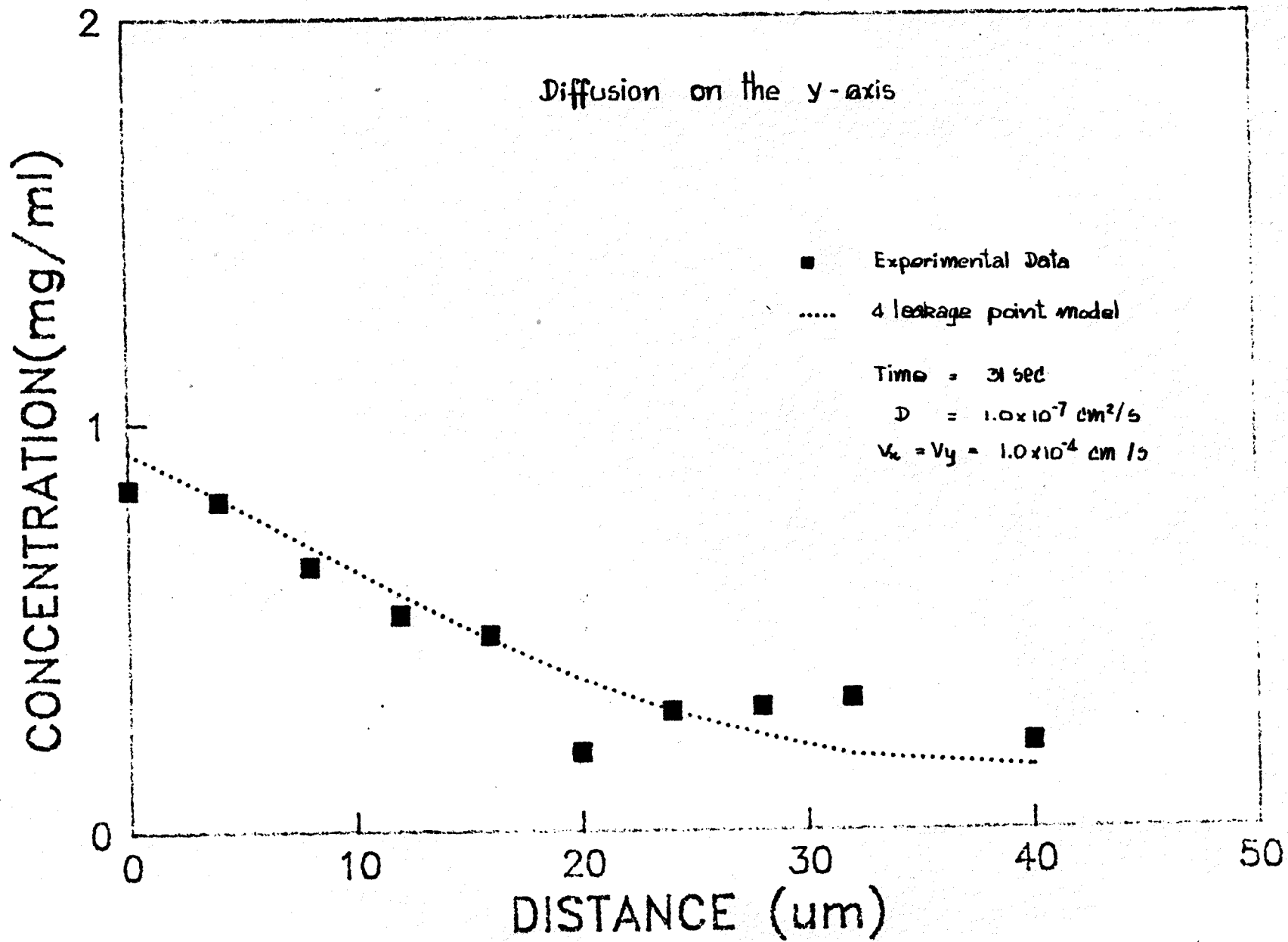


Fig. 4.6a.

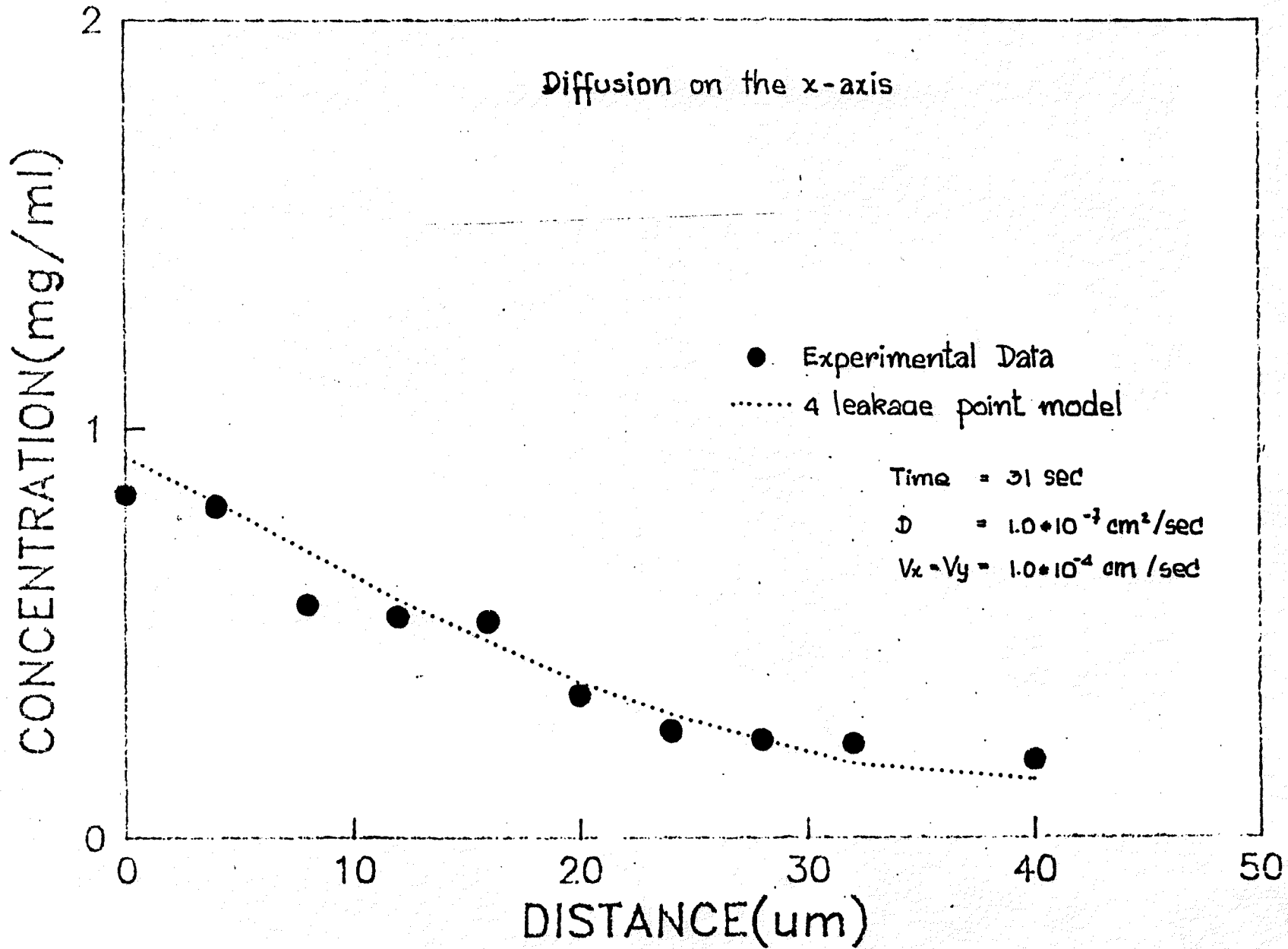


Fig. 4.6.b.

TABLE 4.6.

The position, gray level, and calculated concentration at each pixel (the second subregion from Fig.1.3) used in the graph of concentration vs distance in Fig.4.8.

Y*	X*	X-AXIS Concentration (mg/ml)	Distance (um)
73	16	0.92	0.0
74	15	0.78	4.0
75	14	0.76	8.0
76	13	0.70	12.0
77	12	0.41	16.0
78	11	0.31	20.0
79	10	0.12	24.0
80	9	0.17	28.0
81	8	0.16	32.0
82	7	0.11	36.0
83	6	0.07	40.0

* Diffusion along the lines perpendicular and parallel line to the leaking vessel.

TABLE 4.7.

The solution of the theoretical model used in the graph of concentration vs distance in Fig.4.8.

Distance (μm)	X-AXIS Concentration* (mg/ml)
0.0	1.19
4.0	0.94
8.0	0.74
12.0	0.57
16.0	0.45
20.0	0.34
24.0	0.26
28.0	0.20
32.0	0.15
36.0	0.12
40.0	0.09

* Calculated from the model using the following parameters :
time step = 0.1 , at 310 iterations = $0.1 \times 310 = 31$ sec
initial concentration = 2.39 mg/ml
diffusion coefficient = $10.0 \mu\text{m}^2/\text{sec}$
solvent velocity (V_x, V_y) = $0.1 \mu\text{m}/\text{sec}$, $\Delta x = \Delta y = 4.0 \mu\text{m}$

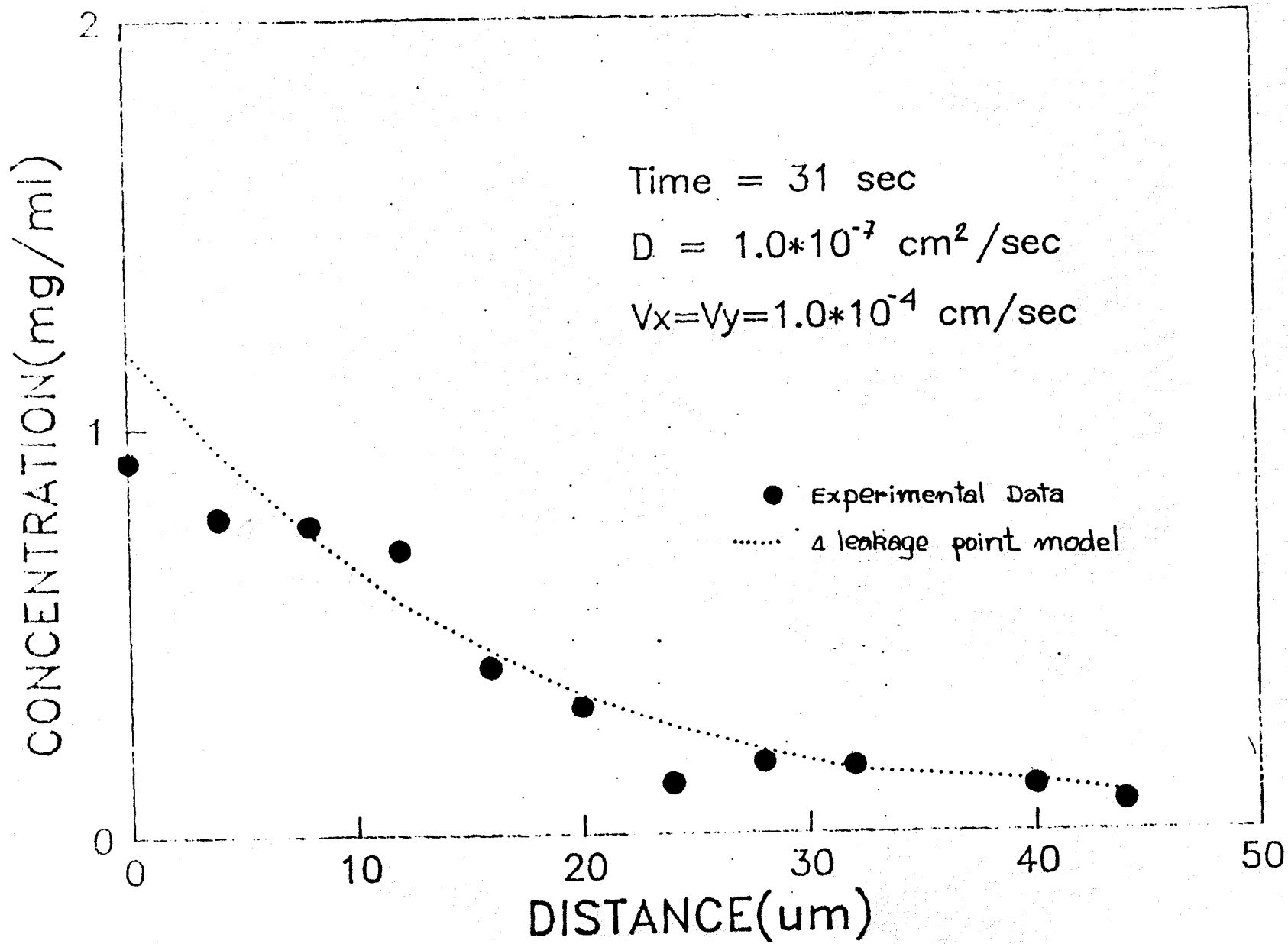


Fig.4.8

DISCUSSION

The Best Fit Model :

The model which best fit the data of the second experiment was a four corner leakage model shown schematically in Fig.4.3. At time zero every point in the 15x15 arrays are zero except the four leakage points; (1,1),(1,2),(1,3),(1,4). Those four points simulated the leakage site in which the FITC-dextran concentration was constant at the concentration of tracer measured in the plasma phase. This assumed that concentration of tracer inside the leaking microvessel was constant during the observation time and the same as that measured in samples taken from large vessels. In the first experiment the gray level distribution during the control time helped to better approximate the initial condition of the leakage area. Figure 5.1 is a plot of concentration vs. distance at 53-sec and 105-sec diffusion times (Fig.1.1,1.2). Figure 5.1 shows that the grayscale (concentration) at point adjacent to the leaking vessel wall were still increasing during 105 second. Therefore, the mean concentration inside the leaking vessel (about 1.36 mg/ml) was used for the steady initial condition in the simulation of the 53-sec data. This observation supported the approximation of constant initial conditions for the simulation of the smaller period of diffusion in the second experiment (31 sec).

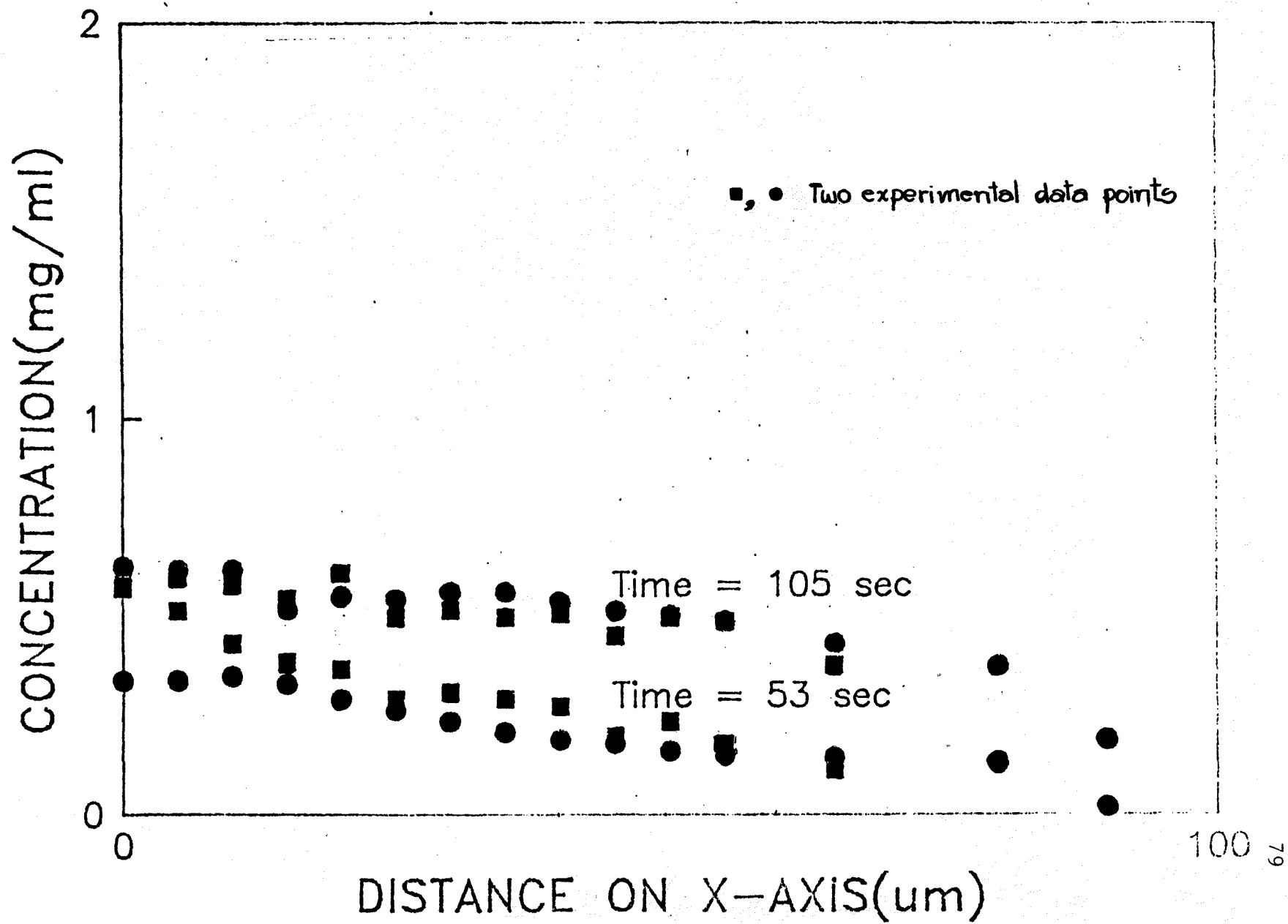


Fig. 5.1.

The number of leakage points in the model which best fit the data were obtained from an analysis of the concentration profiles in Fig.1.1,1.2 for the first experiment. Figure 4.1 shows that five pixels on the vessel wall at the leakage site had almost constant grey levels during the entire diffusion period. It was assumed that they were constant at initial concentration. The five leakage pixels along with the 3 μm between pixels indicated that the length of the leakage area was about $3 \times 5 \mu\text{m}$ border. In the theoretical model this length correspond to four points as the distance used between points was 4 μm .

However since the second experiment only had one concentration profile at 31 sec(Fig.1.3). Details of the leakage pattern could not be explored as much as in the first experiment. In 31-sec diffusion data it was observed that there were also five pixels near the edge of the leaking vessel that had no gray level difference (the result of the subtraction of the control greylevel values produced greylevels near zero in these pixels). Therefore the number of leakage points in the theoretical model could also be four. By trial and error, the results showed that the best fit model was one in which the leakage points were at the corner not at the middle.

Fig.4.4 and 4.8 show that the experimental data always gave a lower values for the concentration at points near the vessel wall on the x-axis than did the solution of

theoretical model. The reason for this can be explained in two different ways. First, some damage of the cells at the vessel wall could have caused the leakage to occur during the control period so that the gray level difference from subtraction of the control values is less than it should be. Second, the diffusion of macromolecules such as FITC-dextran 150 through the vessel wall is effected by the complicated structure of the microvessel wall. The data of Fox and Wayland (ref.6) show that gaps occur when two or more endothelial cells come together to form a position of the vessel wall. Computer reconstruction of the cell junctions showed very complex geometry.

The solution of model with the same model coefficient values could be varied to accommodate a different number of points on the x- and the y- axes. This feature allowed the model to better approximate the heterogenous nature of the actual system. The diffusion of molecules throughout the tissue is confined to limited regions, rather than being uniformly spread throughout the available area. The ultrastructure (ref.5,10) of the interstitial space shows considerable spatial heterogeneity so that one would expect regions of high permeability to macromolecules adjacent to regions of low permeability. From the concentration profiles (Fig.1.1,1.2 and 1.3), the sizes of subregions could be identified and it was assumed that within each subregion the structure was similar from point to point,

so that the concentration gradients only depended on the distance from the leakage site within each subregion. This boundary criteria is described in more detail by Nugent and Jain (ref.12,16) and will be discussed in the following section.

RELATED WORK DONE BY OTHERS

The value of the diffusion coefficient that gave the best fit to the data is an apparent diffusion coefficient for FITC-dextran 150 in the hamster cheek pouch, to distinguish it from the free diffusion coefficient in distilled water extrapolated to infinite dilution, D_0 . The permeability of FITC-dextran (molecular weight of approximately 150,000) in control vessel is negligible. Gerlowski reported that dextran 150 would not appreciably leak into the extravascular space for up to three hours of control in the rabbits ear chamber microcirculation. However, the intravenous injection of histamine increased extravasation of dextran 150 not only in normal tissues but also in tumor tissues.

The value of this calculated apparent diffusion coefficient ($1.0 \times 10^{-7} \text{ cm}^2/\text{sec}$) was less than the one reported by Nakamura (ref.16). Nakamura results, reported in Table 5.1. show an apparent diffusion coefficient of about $2.4 \times 10^{-7} \text{ cm}^2/\text{sec}$ for FITC-dextran 152,700. This was estimated from the integration of the one-dimensional diffusion equation :

$$\partial C(x,t)/\partial t = \frac{\partial}{\partial x} \left[D \left(\frac{\partial C(x,t)}{\partial x} \right) \right]$$

where $C(x,t)$ is the concentration at any distance x , and time, t , and D is the diffusion coefficient.

Nakamura's model did not include an interstitial velocity (convection contribution). In Fig.5.2 we see that at the same D' (1.0×10^{-7} cm²/sec) the concentration at the same distance, at the same time is increased by interstitial velocity (V_x, V_y). A more important reason is that in Nakamura's experiments, it was likely that the tracers passed through the mesothelium and diffused into the water film above and below the tissue itself. Since these aqueous layers were considerably greater in thickness than the tissue, the fluorescent emission from tracers in the aqueous layer would dominate and values of apparent diffusion coefficients would approach the values for free diffusion coefficients.

Nakamura's experiments were done in cat mesentery, and permeability to macromolecules differs from organ to organ. Such differences are consistent with electron microscopic findings of differences in the structure of microvascular walls from organ to organ (ref.16).

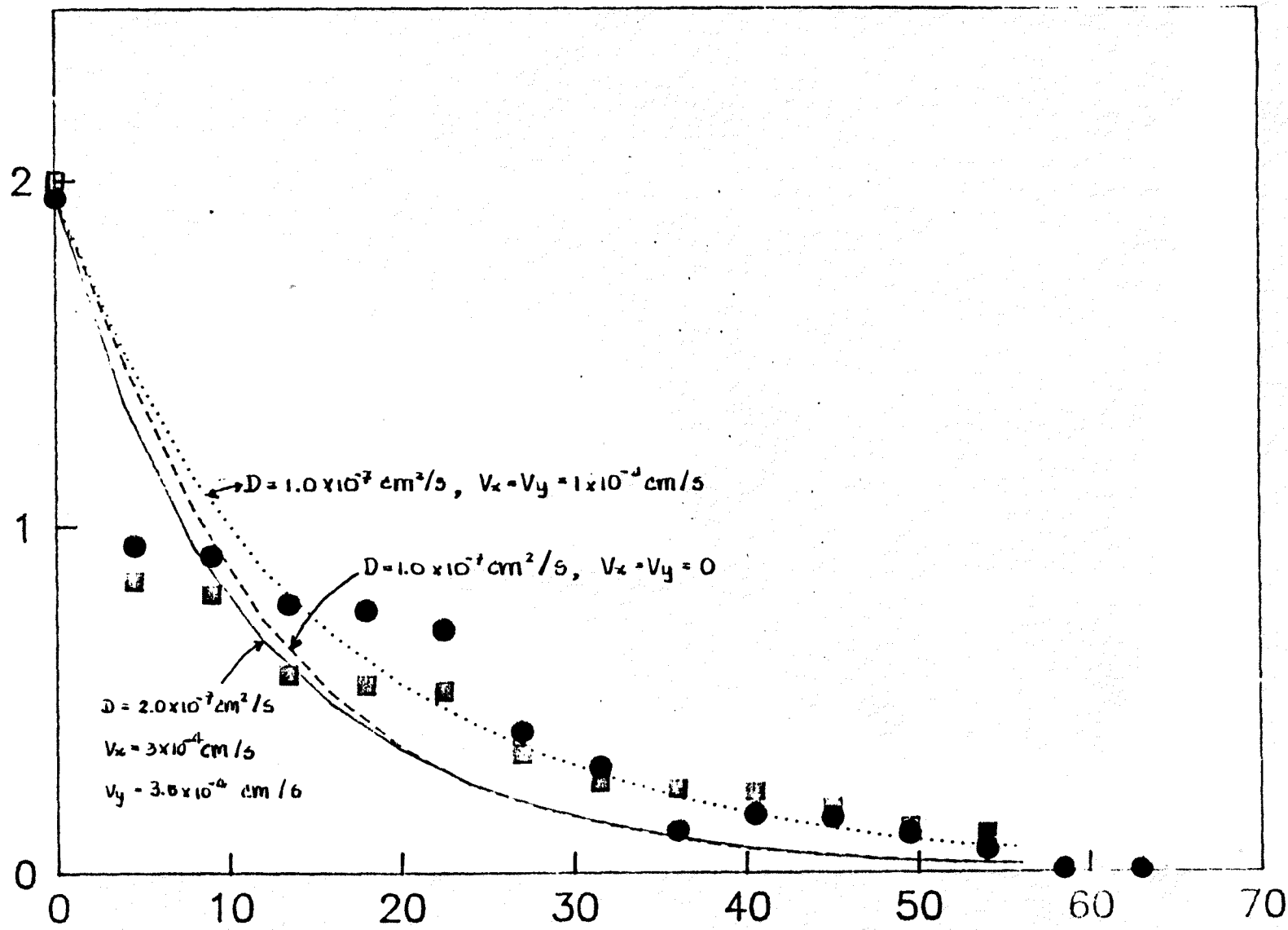


Fig. 5.2.

TABLE 5.1.

Calculated Diffusion Coefficients For Dextrans And BSA
In Mesenteric Reported by Nakamura And Wayland (ref.16).

Species	\bar{M}_w	\bar{M}_n	$D \cdot 10^7$ (cm^2/sec)	
FITC-Dextran	3400	2500	27.0	± 2.5
FITC-Dextran	19,100	17,300	9.3	± 0.3
FITC-Dextran	41,200	28,200	6.7	± 0.4
FITC-Dextran	152,700	101,100	2.4	± 0.3
FITC-Dextran	393,900	166,800	1.7	± 0.1
FITC-BSA	(69,00)		6.4	± 0.5

\bar{M}_w = weight average molecular weight

\bar{M}_n = number average molecular weight

In 1977 the D' of FITC-dextran in rat mesentery (Table 5.2) reported by Fox and Wayland (ref.6) were less than the one calculated from the model in this paper. One reason for the differences in estimated diffusion coefficient is tissue structure (the interstitial matrix of the rat mesentery is extremely dense). Another reason for the difference is the 100-times greater concentration of FITC-dextran 150 used in their experiments. Their dextran 150 had a degree of substitution of 0.01-0.001 FITC molecules / glucose subunit. This range of substitutions would bias their data toward tracer molecules with the greatest deviation in molecular size, shape, charge and other properties from the unlabeled molecule (ref.14,16).

TABLE 5.2.

Apparent Diffusion Coefficients Of Fluorescent Tracers
In Mesentery.

Tracer	$a\bar{M}_w$	$b\bar{M}_n$	$D_o * 10^7$ (cm ² /sec)	$D' * 10^7$ (cm ² /sec)
FITC-Dextran	3,400	2,500	22.9	5.6
	19,100	17,300	10.6	5.9
	19,000	17,500	10.6	2.6
	26,350		36.4	9.1
	35,200	26,000	42.1	7.9
	41,200	28,200	44.9	7.3
BSA-FITC	68,000		34.5	9.5

a \bar{M}_w = weight average molecular weight

b \bar{M}_n = number average molecular weight

D_o = Free diffusion coefficient at infinite dilution

D' = Apparent diffusion coefficient in mesentery

Nugent and Jain (ref.12) modeled their rabbit ear chamber data using a model of one-dimensional diffusion in a semi-infinite medium :

$$\partial C / \partial t = D (\partial^2 C / \partial x^2) \quad (5.1)$$

$$C_{x,0} = 0 \quad (5.2)$$

$$C_{0,t} = f(t) \quad (5.3)$$

$$C_{\infty,t} = 0 \quad (5.4)$$

where $C_{x,t}$ is the test molecule concentration at distance x from a specified origin at time t , and D is the apparent interstitial diffusion coefficient, assumed to be constant. Since the tracer was not present in the extravascular space prior to injection, $C_{x,0} = 0$. The origin was defined at a position just outside the capillary wall ($x=0$) where intensity measurement specifies a time-dependent concentration function, $C_{0,t} = f(t)$. A solution to the system of equations which was applicable for short penetration distances was sought since capillary interactions in long-term data were manifested as deviations in model predictions due to violation of the boundary condition $C_{\infty,t} = 0$. The solution to this system for constant D is readily obtained (ref.12,16)

$$C_{x,t} = 2\pi^{-1/2} \int_{\lambda} f(t-x^2/(4D\mu^2)) e^{-\mu^2} d\mu \quad (5.5)$$

where $\lambda = x/(4Dt)^{1/2}$ and μ is a dummy variable for integration. To develop analytical criteria with which to evaluate the effects of capillary interactions on the data

at a specified position of measurement, a one-dimensional analogue to the Krogh cylinder model was considered. Capillary transport interactions were assumed to be adequately represented by a surface of no-flux at a distance L from the origin. Accordingly, eq.(5.4) is replaced by

$$\partial C_{L,t} / \partial x = 0 \quad (5.6)$$

For a step change in concentration at the origin ($f(t)=C_0$), the deviation between concentration predicted when allowing for capillary interaction (Krogh analog) and that predicted with the assumption of noninteraction approaches 2% at a time

$$t_D = TL^2/D \quad (5.7)$$

where T is a function of x/L which has been approximated by

$$T \approx 0.57 - 1.30(x/L) + 1.14(x/L)**2 \quad (5.8)$$

for $0.1 \leq x/L \leq 0.6$.

Since regions for diffusion measurements had intercapillary distances greater than 100 μm , L was chosen to be 50 μm as a conservative estimate. The iteration time t_D was used as an absolute upper time limit for the application of Eq.5.6. Model predictions (Table 5.3) show excellent agreement with the data obtained over times less than t_D yielding best-fit values of D for the test molecules studied.

TABLE 5.3

Tissue diffusion coefficients in rabbit ear chamber.

Test Molecule	a_E nm	$D_o * 10^7$ cm ² /sec	$D * 10^7$ cm ² /sec
Na-F	0.48	70	20
			24
FITC-D20	3.2	10.2	1.7
			2.3
FITC-D40	4.62	7.11	0.22
			0.18
FITC-70	5.79	5.67	0.048
			0.061
FITC-BSA	3.55	9.3	0.16
			0.11

 a_E = Molecular Radius.

Possible Errors :

1. We do not have a true measure of the concentration at any point, only a measure of the total amount of fluorochrome in each region of the tissue. If the diffusion substance is confined to limited regions, rather than being uniformly spread throughout the tissue, this means that the actual concentration in the aqueous spaces is higher, but if the structure is similar from point to point, the concentration gradients, normalized to value at the arbitrary origin, will be correctly measured.

2. There would be greater interference of tissue elements with the diffusion of the larger macromolecules (lower diffusion coefficients).

3. The theoretical equation was derived for an infinitely dilute, homogeneous, isotropic binary solute-solvent system. Although steric and possibly electrostatic interaction between tracer molecules and other solutes and with the interstitial matrix undoubtedly occur, and although local variation in tracer distribution was observed (similar to patterns reported by McMaster and Parsons (ref.8) and by Wiederhielm (ref.15), eq.(2.8) was applied to a sufficiently large area (about 40 μm along each axis) that any random spatial variation of tissue properties tended to average out, and systematic deviations from ideality were manifested in the value obtained for the diffusion coefficient.

4. Since the initial condition used for the solution of eq.(2.8) was empirically determined. For example in the first experiment control gray-level data was available. Therefore, the initial concentration was approximated as being equal to the mean of the gray level inside the leaking vessel (about 145) and the concentration was calculated as : $145 \times 2.39 / 255 = 1.36$ mg/ml). However in the second experiment the initial concentration was approximated as 2.39 mg/ml, in the absence of control gray level information. This means that no meaningful statistical test could be applied to the calculated values of D' , V_x , and V_y .

In future experiments control values of graylevel should be recorded before each experiment.

CONCLUSION

The low apparent diffusion coefficient for macromolecules such as FITC-dextran 150 which was estimated in this paper suggest that, the interstitial space has a structure which acts as a barrier to free diffusion of large molecules such as proteins. In transient phenomena such as the increase in microvascular permeability observed upon topical applications of vasoactive agents, interstitial concentration gradients would be expected and transport of macromolecules would be effected by the physical-chemical properties of the interstitial matrix.

The apparent diffusion coefficient reported in this thesis should be considered simply as a descriptive parameter that results from the particular model which was formulated using the assumptions listing in the mathematical model section. Further experimentation and improvement of the transport models would be necessary to meaningfully apply these results to draw more detailed conclusions about the physical-chemical properties of the interstitial space which can be related to actual molecular phenomena.

APPENDIX A.

List Of Computer Software :

MAIN PROGRAM

BOU PROGRAM

COEFF PROGRAM

SCONV PROGRAM

&MAIN T=00004 IS ON CR00058 USING 00018 BLKS R=0000

```

0001 FTN66
0002 $FILES(2,1)
0003     PROGRAM MAIN
0004 C -----
0005 C
0006 C     THIS PROGRAM IS MAIN PROGRAM THAT IS USED TO FIND THEORETICAL
0007 C     CONCENTRATION OF DIFUSSING MACROMOLECULES AT EACH TIME STEP,
0008 C     AT EACH GRID POINTS.
0009 C
0010 C -----
0011 C
0012 C
0013     DIMENSION C(21,21),Y(21,21),Z(10),A(10),B(5)
0014     DIMENSION NOEF(10),NONI(10),NOUT(10)
0015     COMMON C,Y,MPON,DT,NEND,K,CB,A,B,N,TN,LPT
0016     COMMON ICO,ICP,IP
0017     LU = LOGLU(LU)
0018 C
0019 C->READ NUMBER OF TIME STEP,TOTAL LOOP COUNTERS,AND TIME STEP
0020 C FOR PRINTING OUTPUT.
0021 C
0022 111  WRITE(LU,1)
0023 1    FORMAT (/"Enter time step size,no.of iterations,K value that "/
0024     2"will print after K time points")
0025     READ(LU,*) DT,NEND,LPT
0026 C
0027 C->READ DIFFUSION COEFFICIENTS,VELOCITIES ON X,Y-AXIS,
0028 C AND REACTION RATES (always zero in this model).
0029 C
0030 7    WRITE(1,10)
0031 10   FORMAT(/"Enter filename that contains coeff. values")
0032     READ (1,30) (NOEF(I),I=1,10)
0033 30   FORMAT (40A2)
0034     OPEN(88,FILE=NOEF,IOSTAT=IOS,ERR=100,STATUS='OLD')
0035     READ(88,*) (A(I),I=1,5)
0036     READ(88,*) (B(I),I=1,3)
0037     CLOSE(88,IOSTAT=IOS,ERR=101,STATUS='KEEP')
0038 C
0039 C->READ INITIAL AND BOUNDARY CONDITIONS
0040 C
0041     WRITE(1,40)
0042 40   FORMAT(/"Enter filename that contains initial&boundary condition")
0043     READ(1,30) (NONI(I),I=1,10)
0044     OPEN(88,FILE=NONI,IOSTAT=IOS,ERR=102,STATUS='OLD')
0045     READ(88,*) CB,MPON,IP,ICO
0046     IF(ICO.EQ.2) ICP=MPON/2
0047     DO 11 I = 1,MPON+1
0048     DO 15 J = 1,MPON+1
0049     READ(88,*) C(I,J)
0050 15   CONTINUE
0051 11   CONTINUE
0052     CLOSE(88,IOSTAT=IOS,ERR=103,STATUS='KEEP')
0053     TN=0.0
0054     L=1
0055     K=1
0056 C
0057 C->ENTER OUTPUT FILENAME
0058 C

```

```

0059      WRITE(1,80)
0060      80  FORMAT(/"Enter filename for output")
0061      READ(1,30) (NOUT(I),I=1,10)
0062      OPEN(88,FILE=NOUT,IOSTAT=IOS,ERR=106,STATUS='NEW')
0063      DO 70 N=1,NEND
0064      TN=DT*FLOAT(K)
0065      CALL RUNGE
0066      DO 25 I=2,MPON
0067      DO 20 J=2,MPON
0068      C(I,J)=Y(I,J)
0069      20  CONTINUE
0070      25  CONTINUE
0071      IF(N .NE. K) GOTO 70
0072      WRITE(88,300) TN
0073      DO 27 I=1,MPON
0074      WRITE(88,401) (C(I,J),J=1,7)
0075      WRITE(88,402) (C(I,J),J=8,13)
0076      WRITE(88,402) (C(I,J),J=14,MPON)
0077      27  CONTINUE
0078      K=LPT*L
0079      L=L+1
0080      70  CONTINUE
0081      CLOSE(88,IOSTAT=IOS,ERR=107,STATUS='KEEP')
0082      C
0083      GOTO 1000
0084      100  WRITE(1,201)
0085      GOTO 1000
0086      101  WRITE(1,202)
0087      GOTO 1000
0088      102  WRITE(1,203)
0089      GOTO 1000
0090      103  WRITE(1,204)
0091      GOTO 1000
0092      104  WRITE(1,205)
0093      GOTO 1000
0094      105  WRITE(1,206)
0095      GOTO 1000
0096      106  WRITE(1,207)
0097      GOTO 1000
0098      107  WRITE(1,208)
0099      201  FORMAT('Error on open file coef')
0100      202  FORMAT('Error on close file coef')
0101      203  FORMAT('Error on open file coni')
0102      204  FORMAT('Error on close file coni')
0103      205  FORMAT('Error on open file boud')
0104      206  FORMAT('Error on close file boud')
0105      207  FORMAT('Error on open file output')
0106      208  FORMAT('Error on close file output')
0107      300  FORMAT(/,33X,'TIME=',E14.8/)
0108      311  FORMAT(A1)
0109      401  FORMAT(/,1X,7(F8.4,2X))
0110      402  FORMAT(1X,6(F8.4,1X))
0111      1000 WRITE(1,321)
0112      321  FORMAT(/'Do you want to do another simulation? Y/N')
0113      READ(1,311) IANS
0114      IF(IANS.EQ.1HY) GOTO 111
0115      STOP
0116      END
0117      C
0118      C

```

```

0119      SUBROUTINE RUNGE
0120      C
0121      C
0122      DIMENSION C(21,21),Y(21,21),Z(10),A(10),B(5)
0123      DIMENSION NOEF(10),NONI(10),NOUT(10)
0124      COMMON C,Y,MPON,DT,NEND,K,CB,A,B,N,TN,LPT
0125      COMMON ICO,ICP,IP
0126      REAL K1,K2,K3,K4
0127      AR=1.-1./SQRT(2.)
0128      BR=1.+1./SQRT(2.)
0129      CR=-0.5+1./SQRT(2.)
0130      DR=-1./SQRT(2.)
0131      DO 2 J=1,MPON
0132      C(MPON+1,J)=C(MPON,J)
0133      2 CONTINUE
0134      DO 3 I=1,MPON
0135      C(I,MPON+1)=C(I,MPON)
0136      3 CONTINUE
0137      DO 15 I=2,MPON
0138      DO 5 J=2,MPON
0139      IF(ICO.EQ.3) GOTO 11
0140      IF(ICO.EQ.2) GOTO 10
0141      DO 6 M=1,2
0142      C(M,ICP)=CB
0143      DO 7 L=1,IP
0144      IC=MPON/2+L
0145      IL=MPON/2-L
0146      C(M,IC)=CB
0147      C(M,IL)=CB
0148      7 CONTINUE
0149      6 CONTINUE
0150      GOTO 11
0151      10 DO 8 L=1,IP
0152      C(1,L)=CB
0153      C(2,L)=CB
0154      8 CONTINUE
0155      11 K1=A(1)*(C(I-1,J)+C(I+1,J))+A(5)*C(I,J)+A(3)*(C(I,J-1)+C(I,J+1))+
0156      2B(1)*(C(I,J)-C(I+1,J))+B(2)*(C(I,J)-C(I,J+1))+B(3)
0157      DK1=(DT*K1)/2.
0158      Z(1)=C(I-1,J)+DK1
0159      Z(2)=C(I+1,J)+DK1
0160      Z(3)=C(I,J)+DK1
0161      Z(4)=C(I,J-1)+DK1
0162      Z(5)=C(I,J+1)+DK1
0163      K2=A(1)*(Z(1)+Z(2))+A(5)*Z(3)+A(3)*(Z(4)+Z(5))+B(1)*(Z(3)-Z(2))+
0164      2B(2)*(Z(3)-Z(5))+B(3)
0165      DK2=DT*(CR*K1+AR*K2)
0166      Z(1)=C(I-1,J)+DK2
0167      Z(2)=C(I+1,J)+DK2
0168      Z(3)=C(I,J)+DK2
0169      Z(4)=C(I,J-1)+DK2
0170      Z(5)=C(I,J+1)+DK2
0171      K3=A(1)*(Z(1)+Z(2))+A(5)*Z(3)+A(3)*(Z(4)+Z(5))+B(1)*(Z(3)-Z(2))+
0172      2B(2)*(Z(3)-Z(5))+B(3)
0173      DK3=DT*(DR*K2+BR*K3)
0174      Z(1)=C(I-1,J)+DK3
0175      Z(2)=C(I+1,J)+DK3
0176      Z(3)=C(I,J)+DK3
0177      Z(4)=C(I,J-1)+DK3
0178      Z(5)=C(I,J+1)+DK3

```



```
0179      K4=A(1)*(Z(1)+Z(2))+A(5)*Z(3)+A(3)*(Z(4)+Z(5))+B(1)*(Z(3)-Z(2))+
0180      2B(2)*(Z(3)-Z(5))+B(3)
0181      Y(I,J)=C(I,J)+(DT/6.)*(K1+2.*AR*K2+2.*BR*K3+K4)
0182      IF(ICO.EQ.3) GOTO 5
0183      IF(ICO.EQ.2) GOTO 12
0184      DO 13 M = 1,2
0185      Y(M,ICP)=CB
0186      DO 14 L =1,IP
0187      IC=MPON/2+L
0188      IL=MPON/2-L
0189      Y(M,IC)=CB
0190      Y(M,IL)=CB
0191      14 CONTINUE
0192      13 CONTINUE
0193      GOTO 5
0194      12 DO 16 L=1,IP
0195      Y(1,L)=CB
0196      Y(2,L)=CB
0197      16 CONTINUE
0198      5 CONTINUE
0199      15 CONTINUE
0200      RETURN
0201      END
```

```

&BOU T=00004 IS ON CR00058 USING 00005 BLKS R=0000

0001 FTN66
0002 $FILES(2,1)
0003 PROGRAM BOU
0004 C
0005 C -----
0006 C THIS PROGRAM DEFINED BOUNDARY AND INITIAL CONDITION
0007 C -----
0008 C
0009 COMMON LU
0010 DIMENSION C(21,21),NAME(10),IL(21),IC(21)
0011 LU=LOGLU(LU)
0012 WRITE(LU,1)
0013 1 FORMAT(/"Enter initial concentration,even number of points"/
0014 1"on each axis and odd number of leakage points.")
0015 READ(LU,*) CB,MPON,IP
0016 DO 5 I=1,MPON+1
0017 DO 6 J=1,MPON+1
0018 C(I,J)=0.0
0019 6 CONTINUE
0020 5 CONTINUE
0021 WRITE(LU,20)
0022 20 FORMAT(/,"Choose one choice for model,please (1,2,3)"/
0023 1" 1.Middle leakage points "/
0024 2" 2.Corner leakage points "/
0025 3" 3.Every points on line")
0026 READ(LU,*) ICO
0027 IF(ICO.NE.3) GOTO 25
0028 DO 22 J=1,MPON+1
0029 C(1,J)=CB
0030 22 CONTINUE
0031 GOTO 39
0032 25 IF(ICO.EQ.2) GOTO 30
0033 IP=(IP-1)/2
0034 ICP=MPON/2
0035 DO 33 I =1,2
0036 C(I,ICP)=CB
0037 DO 35 L=1,IP
0038 IC=MPON/2+L
0039 IL=MPON/2-L
0040 C(I,IC)=CB
0041 C(I,IL)=CB
0042 35 CONTINUE
0043 33 CONTINUE
0044 GOTO 39
0045 30 IP=IP+1
0046 DO 37 L =1,IP
0047 C(1,L)=CB
0048 C(2,L)=CB
0049 37 CONTINUE
0050 39 WRITE(1,105)
0051 105 FORMAT(/"Enter filename for output file")
0052 READ(1,80) (NAME(I),I=1,10)
0053 80 FORMAT(40A2)
0054 OPEN(88,FILE=NAME,IOSTAT=IOS,ERR=202,STATUS='NEW')
0055 WRITE(88,*) CB,MPON,IP,ICO
0056 DO 50 I=1,MPON+1
0057 DO 45 J=1,MPON+1
0058 WRITE(88,*) C(I,J)

```

```
0059 45 CONTINUE
0060 50 CONTINUE
0061      CLOSE(88, IOSTAT=IOS, ERR=203, STATUS='KEEP')
0062      GOTO 500
0063 202 WRITE(1,300)
0064      GOTO 500
0065 203 WRITE(1,301)
0066 300 FORMAT('Error on open file')
0067 301 FORMAT('Error on close file')
0068 500 STOP
0069      END
```

&COEFF T=00004 IS ON CR00058 USING 00004 BLKS R=0000

```

0001 FTN66
0002 $FILES (2,1)
0003     PROGRAM COEFF
0004 C
0005 C -----
0006 C     THIS PROGRAM CALCULATES COEFFICIENTS FOR MODEL EQUATIONS
0007 C -----
0008 C
0009     DIMENSION A(10),NCOEF(10),B(5)
0010     LU=LOGLU(LU)
0011     5 WRITE(LU,10)
0012     10 FORMAT(/"Enter difussion coef,Dx,Dy,Vx,Vy and Reaction rate")
0013     READ(LU,*) D,DX,DY,VX,VY,RA
0014     A(1)=D/(DX**2.)
0015     A(2)=2.*A(1)
0016     A(3)=D/(DY**2.)
0017     A(4)=2.*A(3)
0018     A(5)=-(A(2)+A(4))
0019     B(1)=VX/DX
0020     B(2)=VY/DY
0021     B(3)=RA
0022     WRITE(1,20)
0023     20 FORMAT(/"Enter filename for coef. values")
0024     READ(1,30) (NCOEF(I),I=1,10)
0025     30 FORMAT(40A2)
0026     OPEN(88,FILE=NCOEF,IOSTAT=IOS,ERR=50,STATUS='NEW')
0027     WRITE(88,*) (A(I),I=1,5)
0028     WRITE(88,*) (B(I),I=1,3)
0029     CLOSE(88,IOSTAT=IOS,ERR=55,STATUS='KEEP')
0030     GOTO 60
0031     50 WRITE(1,51)
0032     GOTO 65
0033     55 WRITE(1,56)
0034     51 FORMAT('Error on open file coef')
0035     56 FORMAT('Error on close file coef')
0036     GOTO 65
0037     60 WRITE(1,61)
0038     61 FORMAT(/,'Do you want to do another calculation? Y/N')
0039     READ(1,62) IANS
0040     62 FORMAT(40A2)
0041     IF(IANS.EQ.1HY) GOTO 5
0042     65 STOP
0043     END

```

&SCONV T=00004 IS ON CR00058 USING 00012 BLKS R=0000

```

0001  FTN66
0002  $FILES(0,4,24)
0003      PROGRAM SCONV
0004  C
0005  C -----
0006  C   THIS PROGRAM WILL CHANGE GREY LEVEL TO CONCENTRATION.
0007  C -----
0008  C
0009      COMMON LU
0010      DIMENSION JARRY(170),CEAK(170),IDATA(10),IANS(10)
0011      LU=LOGLU(LU)
0012      WRITE(LU,10)
0013  10      FORMAT(/"Enter LX,LY:  _")
0014      READ(LU,*) ILXX,ILYY
0015      WRITE(LU,30)
0016  30      FORMAT(/"Enter data filename:  _")
0017      READ(LU,35) (IDATA(I),I=1,3)
0018  35      FORMAT(3A2)
0019      OPEN(70,FILE=IDATA,IOSTAT=IOS,ERR=101,STATUS='OLD')
0020      WRITE(LU,57)
0021      READ(LU,*) CONI
0022      WRITE(LU,60)
0023  57      FORMAT(/"Enter initial concentration:  _")
0024  60      FORMAT(/"Enter output filename:  _")
0025      READ(LU,35) (IANS(I),I=1,3)
0026      OPEN(71,FILE=IANS,IOSTAT=IOS,ERR=103,STATUS='NEW')
0027      REWIND 70
0028      DO 85 L=1,ILYY
0029      DO 80 J=1,ILXX,5
0030          J1=J+1
0031          J2=J+2
0032          J3=J+3
0033          J4=J+4
0034      READ(70,*) J,I,JARRY(J),J1,I,JARRY(J1),J2,I,JARRY(J2),J3,I,
0035      1JARRY(J3),J4,I,JARRY(J4)
0036      CEAK(J)=(JARRY(J)*CONI)/255
0037      CEAK(J1)=(JARRY(J1)*CONI)/255
0038      CEAK(J2)=(JARRY(J2)*CONI)/255
0039      CEAK(J3)=(JARRY(J3)*CONI)/255
0040      CEAK(J4)=(JARRY(J4)*CONI)/255
0041      WRITE(71,207) J,I,CEAK(J),J1,I,CEAK(J1),J2,I,CEAK(J2),J3,I,
0042      1CEAK(J3),J4,I,CEAK(J4)
0043  80      CONTINUE
0044  85      CONTINUE
0045      CLOSE(70,IOSTAT=IOS,ERR=102,STATUS='KEEP')
0046      CLOSE(71,IOSTAT=IOS,ERR=104,STATUS='KEEP')
0047      STOP 0001
0048  101     WRITE(LU,201)
0049  201     FORMAT('Error on open file')
0050      STOP 0002
0051  102     WRITE(LU,202)
0052  202     FORMAT('Error on close file')
0053      STOP 0003
0054  103     WRITE(LU,203)
0055  203     FORMAT('Error on open file')
0056      STOP 0004
0057  104     WRITE(LU,204)
0058  204     FORMAT('Error on close file')

```

```
0059 207  FORMAT(5(I3,1X,I3,1X,F5.3,1X))  
0060      END
```

REFERENCE

1. Bird, R.Byron , Warren E.Stewart and Edwin N.Lightfoot. The Equations of Change for Multicomponent System. Transport phenomena. Department of Chemical Engineering University of Wisconsin. John Wiley & Sons, Inc. New York. 1960. 558-559.
2. Brice Carnahan , H.A. Luther and James O.Wilkes. Runge-Kutta Methods; Applied Numerical Methods. John Wiley & Sons, Inc. New York. 1969. 361-366.
3. Crank, J. The Mathematics of Diffusion. Oxford University Press. 1975. 2, 141-144.
4. Curry, F.E. , V.H. Huxley and R.H. Adamson. Permeability of single capillaries to intermediate-sized colored solutes. Amer. J. Physiol., 1983, 245, H495-H505.
5. Debora, M. Gawlowski, Arthur B. Ritter and Walter N. Duran. Reproducibility of Microvascular Permeability Responses to Successive Topical Applications of Bradykinin in the Hamster Cheek Pouch. Microvascular Research, 1982, 24, 354-363.
6. Fox, J., F. Galey and H. Wayland. Interstitial diffusion of macromolecules in the rat mesentery. Microvascular Research, 1979, 18, 255-276.
7. Jensen, V.G. and G.V. Jeffreys. Mathematical Methods in Chemical Engineering. Academic Press , New York, 1977, 410-424.
8. McMaster, P.D. and Parsons, R.J. Physiological conditions existing in connective tissue. J. Exp. Med., 1939, 69, 247-264.
9. Nugent, L.J. and Jain,R.K. Plasma pharmacokinetics and interstitial diffusion of macromolecules in capillary bed. Amer. J. Physiol., 1982, H129-H136.
10. Nugent, L.J. Diffusional transport of macromolecules in normal and neoplastic tissues. PhD. thesis, Carnegie-Mellon University, 1982.
11. Nugent, L.J. and R.K. Jain. Interstitial diffusion of macromolecules in normal and tumor capillary beds. AIChE Symposium Series, 1983, In Press.

12. Nugent, L.J. and R.K. Jain. Monitoring transport in the rabbit ear chamber. *Microvascular Research*, 1982, 24, 204-209.
13. Nugent, L.J. and Jain, R.K. Two-compartment model for plasma pharmacokinetics in individual blood vessels. *J. Pharm. Biopharm.*, 1984, 12, 451-460.
14. Nugent, L.J. and Jain R.K. Pore and fiber-matrix models for diffusive transport in normal and neoplastic tissues. *Microvascular Research*, 1984, 28, 270-274.
15. Wiederhielm, C.A. Transcapillary and interstitial transport phenomena in the mesentery. *Fed. Proc.*, 1966, 25, 1789-1798.
16. Yasushi Nakamura and Harold Wayland. Macromolecular transport in the cat mesentery. *Microvascular Research*, 1975, 9, 1-21.